

Author Response to Reviewer Comments
Hydrol. Earth Syst. Sci. Discuss., doi:10.5194/hess-2016-559, 2016.

First and foremost, we would like to thank the reviewers for donating their time to review our manuscript and for providing a fair and constructive review of our work. Our response to general and specific comments is documented below, and reflected in a tracked-version of the revised manuscript.

Based on the general and specific comments below, we focused on improving the introduction, discussion and conclusions. We have revised our problem statement and provided a clearer definition of the scientific objectives as they pertain to the general conceptual model and the style of our geophysical measurements. Our discussion of the geophysical results and its significance to the hydrologic community has been improved by better integrating our interpretation of the various data sets, thereby strengthening our general scientific contributions in the conclusion. Individual reviewer comments have been addressed in the manuscript where necessary. Although some of the technical issues associated with the source of measurement errors in our resistivity method remain an inherent limitation in our survey design, we believe that our approach was reasonable given the site conditions and research objectives; we have provided a thorough explanation of all comments below.

All author responses refer to the revised tracked version of the manuscript, while reviewer comments (i.e., line numbers) refer to the original submission.

Reviewer 1: General Comments

The study deals with fractured sedimentary bedrock riverbeds and its spatio-temporal groundwater surface water exchange of the Eramosa River within the Grand River Watershed, Ontario, Canada. Surface electrical methods (ERT and EMI) were used for a quasi non-invasive assessment of the scale and temporal variability of riverbed temperature and groundwater surface water exchange beneath its sedimentary bedrock riverbed. Underpinned were the solid geophysical data sets by a network of boreholes and streambed piezometers, installed across the site. The study further contained highly relevant material for HESS, is well written, structured and cited and attested the authors' fundamental background and experiences with the selected topic. Fractured sedimentary bedrock systems and its interaction processes are very complex and difficult to describe. Hence the presented study provided a useful approach for cost-efficient investigation into the river flow regime. Still there are a few issues that needs to be addressed until the manuscript is ready for publication. Although the study impressed be the amount of high quality data and different applied methods, it lacks a little of a clear and comprehensive purpose.

Response: We have revised the introduction to highlight the state of the science, identify the specific research needs, and outline the specific contributions of our study adds to the conceptual model. We also incorporated more specific details regarding the regional groundwater flow system.

Studies of interaction flow processes at rivers are relatively common since about one decade; however, the presented geophysical investigation of bedrock rivers combined with ground truths core data is unique. Moreover, the economic and ecological potential of global bedrock rivers are remarkable, hence the study can be considered as a pioneer study with portable conclusions. This seems the strengths of this study, however it needs to be emphasized.

Response: We have provided a more detailed summary of the unique contributions of this study in the introduction (Lines 183-196) and its relevance to a broader environmental audience. A similar emphasis was implemented in the final paragraph of the conclusion section.

It would be helpful if the authors establish somehow a relation between their investigations and findings, and a direct affected related system, such as a water supply or ecosystem services. If not available for the selected test site then relevant literature can be used. In this respect the manuscript might be slightly rearranged. Introduction should contain a clear state of the art containing the situation, the problem, the challenge and the provided response (solution).

Response: The basic conceptual model of a groundwater-surface water mixing zone in a fractured bedrock river is now presented in the introduction. The mechanisms controlling this exchange are explained using the conceptual model (Fig. 1) in light of related literature. This is followed by an explanation of our study approach and motivation, along with the specific challenges and the anticipated contributions of this work. Refer to Lines 142-196.

Although I like the extra paragraph 2 ‘background’, it’s quite uncommon and could be incorporated into the introduction and the material and method part, respectfully. It is always helpful to read what other studies have archived at similar test sites and / or with similar approaches and where they were limited. This should be highlighted in the introduction and in the conclusion (and in the abstract too).

Response: We have re-arranged the background section. The literature review is now presented in the introduction (Lines 82-141).

The conclusion should hence contain the extracted information given by the findings as kind of a ‘take home message’ for the scientific community rather than a second abstract. I recommend acceptance with minor revision.

Response: We have revised the conclusion section to better highlight the specific conclusions of this study. The first paragraph provides an overview of the work. The second and third paragraphs provide the specific contributions. The fourth and final paragraph explains the impact and relevance of this study to a broader scientific community.

Specific Comments:

Line 94 – 96: amount of references can be decreased by a related review

Response: We have maintained the original citation list.

Line 126: please mention that the presented Archie’s law is simplified are provide the whole equation

Response: We have added “a fluid saturated medium” to identify the simplified form of this equation (Lines 498). We did provide additional text regarding the underlying assumptions of this equation (Lines 503-506).

Line 144: just mentioned the temperature correction was done by Arps (1953) might be sufficient

Response: Since this equation was used to assess the influence of temperature on the bulk formation resistivity we think it would be best to provide the equation. This equation and associated discussion is now provided in the Methods section (Line 513-522).

Line 224: indicate the approx. location of the EMI lines in Figure 2

Response: Figure 2 has been updated to show the extent of the EMI survey area.

Line 270: use 'Fig' or Figure either but consisted

Response: The full word should be used at the beginning of a sentence but abbreviated in-line.

Line 291: matrix porosities from the corehole relatively low in respect to? A short reference value for the same rock material from the literature is useful or do you mean in comparison to the weathered or broken rubble zone? If so, please mention it

Response: For simplicity we have removed the phrase "...were relatively low" as we do not compare these values to other samples.

Line 321: see above

Response: No further response.

Line 328: it is hard to follow here or maybe I missed the point how you ended up with the 46%, according to Archie in Eq.1? How do you get the Sigma w values or am I totally off? If you re-arrange the equation it needs to be mentioned if not showed

Response: We have modified the wording in the body (Lines 737-769) and the figure caption (Lines 1576-1583). Figure 7 shows the range in formation resistivity based on measured pore water EC (the plot shows effects specific conductance variations and the calculated influence of temperature). Given that water temperature is dynamic and will influence the formation resistivity, we have also provided the potential effect of temperature fluctuations on the formation resistivity. This effect is shown by the bounding isotherms for both groundwater and surface water. The % change in formation resistivity represents the maximum change based on the potential temperature range (e.g., 4-14°C or 0-18°C).

Line 332 – 349: how could you be sure that the EMI data were not affected by outside conditions, do you temperature corrected the ECa as well?

Response: Assuming the reviewer is referring to atmospheric temperature effects on the instruments performance, we do not believe, nor does the manufacturer report that ECa measurement accuracy of the EM-31 (+/- 5% at 20 mS/m) would have any meaningful effect on the reading. The ECa measurements we report in Figure 8 are, of course, sensitive to the temperature of the media as indicated by Eqn 2 and illustrated in Figure 7. ECa variations in the rock are expected to be associated with either temperature fluctuation or specific conductance. Temperature fluctuations within the rock have been used as a tracer to map a zone of influence or transience below the riverbed by other workers. The differences identified in this study could be associated with changes in seasonal groundwater-surface temperature, mixing or changes in groundwater chemistry. The data we present identifies measurable changes in the geoelectrical conditions beneath the riverbed, whether it's due to temperature, EC or some combination of the two; regardless, the spatial extent of these dynamics could support the existence of a mixing zone or simply a zone of thermal variability in the rock unique to this type of river.

Line 420: I prefer including of the discussion together with the presentation of the results. This helps to shorten the manuscript which is almost every time helpful

Response: We appreciate the reviewer's suggestion. Considering the nature of the discussion in this paper we felt it best to separate it from the results to avoid potential confusion (i.e., geophysical results vs. hydrogeophysical interpretation). At this point we have maintained a separate results and discussion section.

Line 857: since you presented the ERT results in Figure 11 by common scale, Figure 10 is kind redundant, mention in the text that the ERT data quality (RMSE, removed data points) were higher under frozen, partly frozen conditions

Response: While we understand the reviewer's comment, we believe the information presented in Fig. 10 is highly informative and critical to the interpretation of the selected data sets in the subsequent figures. The study does contain an immense amount of information, which cannot be presented or summarized in its entirety, but the seasonal trends need to be captured so that reader can fully appreciate the highlighted information. The unique field conditions resulted in many challenges in data processing and interpretation that are best emphasized in Figure 10 rather than hidden or ignored entirely. To our knowledge, there has been no similar study performed in a river in this type of environment, let alone a bedrock rock river, so we think it is critical to provide as much of the data, as possible, particularly if they provide insights into the modelling results.

Reviewer 2: General Comments

This manuscript is on the topic of geophysical and traditional measurements of a reach of river to investigate the suitability for time lapse ERT to study river bottom processes. The writing is in clear, good English, and the figures are mostly very readable and nicely drafted. The topic – either from the Hydrology or Geophysics perspective – certainly has the potential to be of interest to HESS readership. I believe the topic of this work fits into the scope of this journal. The most significant limitation I see to this work is related to the experimental design, which is largely absent from the writing. In short, it is difficult to tell what was being tested about the hydrology, and why measurements were implemented to carry out that test. The stated hypothesis is apparently related to “will the geophysics work,” while the theme of riverbed processes appears and disappears throughout the manuscript. In the end, I remained confused about exactly what the reader was meant to take away from this given the setup of the writing and the design of the study. There is certainly lots of good data here and on some level this has the potential to be of high interest to the hydrology community, but there is a need for substantial revision for focus.

Response: We very much appreciated the reviewers' assessment here. We have made substantial revisions to the introduction, specifically relating to the basic conceptual model (motivation) and the examination of mechanisms controlling groundwater-surface water exchange (hypotheses). The model is now presented in light of existing literature to show the value of our study and provide a clearer description of our study design and elements of the conceptual model we aim to address. The objectives of this study have been re-emphasized and are now more specific to the experimental design/style of measurements collected (Refer to Lines 142-182). Similar changes to the text were implemented in the Conclusion section.

There were several other notable issues/limitations related to measurement methods, data processing, and absence of some measurements that are detailed in my General and Line-by-line comments below. At this time I am recommending this manuscript be returned for major revision, however if the experimental design is not substantially clarified and the focus reworked to highlight hydrological interpretations, a second review would likely not result in a favorable recommendation.

There is a substantial disconnect between the topic of the science question and the posed hypotheses. Although the science question is not explicitly stated, it is my best interpretation that the following reflects the intent of inquiry: “. . . there remain gaps in our conceptual understanding of groundwater-surface water interaction and exchange mechanisms in bedrock rivers where discrete fracture networks will dominate groundwater-surface water flux with secondary interactions supported by the porous rock matrix.” On the other hand, the hypothesis is explicitly stated, although it appears to be limited to a yes-or-no “will it work” type of speculation: “we hypothesize that a groundwater-surface water mixing zone – encompassing fracture and matrix flow and diffusion – may be identified within a fractured bedrock riverbed by monitoring spatiotemporal changes groundwater temperature and porewater electrical conductivity using minimally invasive electrical resistivity methods.” Further complicating matters is the text between Line 69 and 76 that highlight the hydrological outcomes while disregarding the stated hypothesis.

Response: We acknowledge that there are inherent limitations in our study some of which could have been addressed given the benefit of hindsight. We also understand that this study represents a step toward the advancement of the conceptual model. We describe the physical processes with a simple conceptual model based on existing literature from alluvial river studies and fractured sedimentary rock. Our hypothesis was that surface geophysical measurements, specifically electrical methods, may be used to detect changes in geoelectrical properties beneath a bedrock riverbed; this hypothesis was derived from the success of similar studies in alluvial rivers, yet it has never been tested. Therefore, we designed a long-term seasonal resistivity monitoring program, complemented by continuous measurements of groundwater-surface water temperature and EC, to test this hypothesis. In our case, we were able to explore a range of seasonal conditions (including freeze-thaw) and their impact on the bulk electrical properties of the rock. Given that no previous geophysical (or hydrological) studies had been conducted in a bedrock river we did not know *a priori* the effectiveness of our geophysical approach particularly in a hydrological context. In the end, the experiment was successful from the perspective of appreciating the capabilities and limitations of these geophysical methods. Given the benefit of hindsight, we acknowledge that our experiment could have been designed differently or in a way that would have allowed us to examine a different set of questions, such as source of measurement errors and their impacts on the inverse models. That being said, we believe our approach was reasonable given our primary desire to achieve the highest signal-to-noise ratio. Further, comments on this topic are provided below.

Throughout the manuscript, speculative statements about river ice, river-bottom ice and frost are made, though they do not appear to be supported by any direct measurements or observations. Estimates of loss along reaches based on calculations of discharge using rating curves in conjunction with stage height monitoring appear to be absent. This line of evidence would substantially help to support geophysical observations.

Response: We have improved the clarity of our statements regarding river and basal ice. While these features were not directly measured they were observed and did have an impact on our results and interpretation. We also acknowledge the value of monitoring river loss-gain along the reach as this would be helpful in understanding local areas of discharge or recharge in relation to the geophysical measurements; unfortunately this information was not collected in a way (i.e., period and sampling frequency) that would be useful in a direct way to interpret the geophysical dynamics. However, we would like to point out that this data was collected and will be examined in a future paper, at which point, it can be compared to the results of this study.

I felt that the following questions posed early on in the manuscript were not clearly answered: Do you find that groundwater-surface water interaction was restricted by poor vertical connectivity and limited bedrock incision? Did you find that groundwater-surface water connectivity through discrete fractures

was highly variable in space and time, and depended on fracture size or aperture, river stage, and the distribution of hydraulic head within the flow system?

Response: We have revised the questions posed in the introduction to be more representative and consistent with the measurements and observations in this experiment. While these fundamental questions regarding the nature of groundwater-surface water remain, our conclusions are now more reserved given the inherent limitation of geophysical measurements, and absence of direct hydrological information such as groundwater discharge and recharge along the river. The nature of groundwater temperature fluctuations beneath the riverbed remains a central theme of this work.

There is a huge amount of data contained in this manuscript, however in some cases data was left unused in interpretations and discussion. For example, precipitation & snowfall, daily river stage, fracture content as a function of depth, atmospheric temperature, etc. Why include these data if they are not utilized? In the end, if the hypothesis was to test “will ERT work for this” I think that was not clearly answered, and furthermore, given the high dependence on temperature, it may be that that answer is “no.”

Response: Precipitation and weather data provide critical context for the reader and the geophysical measurements we discuss; they also support elements of the conceptual model including thermal zones of influence and the fact that groundwater and surface water can reside in different temperature regimes. Our discussion and interpretation of seasonal transients in the geophysical measurements implicitly utilizes the hydrological information from the perspective of seasonal temperature, precipitation events and river stage fluctuations. We have implemented a number of revisions throughout the manuscript to strengthen the link between atmospheric information and the geophysical measurements.

It should be noted that temperature was viewed as a possible tracer in the delineation of a groundwater-surface water mixing zone; this was motivated from an extensive body of literature utilizing temperature fluctuations to estimate groundwater discharge in rivers (e.g., Lines 121-127). One of our primary goals was to evaluate the relative magnitude of temperature effects on formation resistivity relative to other parameters such as specific conductance and phase transformation. In this case, our study was very successful in identifying the dominance and spatial extent of seasonal temperature transience beneath the riverbed. The mechanisms governing those transience (e.g., fracture aperture, connectivity etc.) will be examined in future work, and will ideally capitalize on the results of this study.

Specific Comments:

Line 55: Perhaps add a comment on what Fan et al., 2007 found here?

Response: Additional details have been added on Lines 76-79.

Line 63: There is a lot going on in the figure and it is weakly linked to the text. Are you testing these concepts?

Response: The conceptual Figure 1 serves as a point of reference and source of motivation for this study. It was not our intent to explicitly test and confirm the various elements described in the model, but rather to illustrate their existence and likely contribution to geoelectrical transience beneath the riverbed. We have improved the placement of the conceptual model in the instruction along with pertinent literature and discussion; we also provide a better description of its relevance to this study. The basic concept we wanted to test was whether or not there was an exploitable geophysical signature, and explore the factors or mechanisms controlling these responses. This would provide at first-order understanding of the geoelectrical response and seasonal transience characteristic of fractured bedrock rivers.

Line 92: The Singha paper has 2014 printed on top of it, but I'm not sure which date is correct.

Response: Based on our records the paper was published on-line in 2014 but wasn't fully published until 2015.

Line 175 – 180: Was the formation of basal ice actually observed at the site or only inferred?

Response: Basal ice was visually observed in the field as indicated in the manuscript. The ice was no longer visible once the river froze over. We have modified the text throughout to clarify this point.

Line 213 – 216: I am unfamiliar with this method of sampling temperature while the sensor is in motion. Certainly the sensor itself, however small it might be, has some thermal mass that requires time to equilibrate to the surrounding water temperature. Even though the sensor is capable of measuring at 0.5 s rate, that does not mean that the measured data are reflecting changes in the formation at that rate. A reliable reference should be included here to justify the method, and a controlled validation test and sensor calibration under laboratory conditions should be conducted to quantify sensor response.

Response: This temperature trolling method has been published by other workers (e.g., Pehme et al. 2010; Pehme et al. 2014, Lines 717-721). However, in this study we utilize a different sensor deployed in a slightly different fashion. The basic approach and resulting data sets are the same.

With respect to the sensor's sampling frequency we can say that these *RBRsolo*TM sensors (RBR Limited, Ottawa, Canada) resolve 63% of a "full-scale" temperature change in 1 s, 95% in 1.5 s and 99% in 2 s. This particular sensor has a maximum resolution of 0.00005°C (full-scale) based on our communications with the manufacture. In this study, we report temperature changes to the nearest 0.01°C. Given our reported rate of decent ~0.8 cm/s combined with our temperature resolution, a conservative vertical "averaging" estimate might be ~1.5 cm based on the full resolution. Therefore, sensor response time in this case appears to be very small and negligible on the data sets presented. Unfortunately, we do not have the laboratory equipment to make any further comments on the performance of this sensor deployed in this way.

We have incorporated additional details on Lines 569-570 to explain the sensors sensitivity and response time.

Line 219: What is the value of measuring snowfall accumulation if snow density is not also reported with a conversion to SWE?

Response: Snow accumulation is reported as SWE. Clarification of SWE has been incorporated into the figure caption on Line 1548-1549.

Line 221/Figure 4: What scale are the red dot "Resistivity Samples" on? They appear to be only temporal and unitless, however they seem to track the river stage which is confusing. Is 'snowfall' in this figure converted to SWE? If not, please do and clarify the label.

Response: The resistive samples "red dots" are plotted in Figure 4 to show their temporal position and sampling interval during the seasonal hydrological conditions. In this case, they track the river stage (y-axis) because these measurements were collected in the river and the stage is explicitly used in the models. Although this could be viewed as unconventional we think this is easiest way to present the data. We have revised the caption of Figure 4 to resolve any potential confusion on the meaning of the red dots.

Line 228: “effective sensing depth” does this mean measurements are reflective of the 6m depth zone, or the entire aggregated zone 0 to 6m depth?

Response: The instruments sampling depth (volume) is defined by a non-linear impulse response function; the sampling depth or interval is dependent on the coil separation and orientation of the induced field. This information can be found in McNeil (1980). Here, the sampling depth is stated as 6 m which is a general rule-of-thumb to the depth of investigation for the instrument in this orientation. We have added “cumulative depth” on Line 588.

Line 237: “BLANKED by bedrock rubble” I am not familiar with this usage of “blanked” in this context. Suggest rewording for clarity.

Response: The word was “blanketed” but we have changed the word to “covered” to avoid confusion.

Line 239 – 244: Does the electrode construction method have any particular importance to this study? This sounds like very typical ERT cable construction, albeit by the end-user rather than a professional fabricator. Probably could be deleted.

Response: In theory the construction of our cables is similar to commercial systems, but because it isn't a commercially available cable we felt it was best to include the details of its construction; some of the design element are unique, which some readers may want to know. Our inclusion of the design of our cable is consistent with the approach of other workers (e.g., Van Dam et al. 2014, Water Resources Research).

Line 261: How was the measurement time determined? It is known that diurnal fluctuations in stream water temperature may be of magnitude in excess of 10C, similar to your annual range of groundwater temperatures. Also you acknowledge the affect of temperature on the ERT readings; how does the timing of the measurements affect the data due to daily fluctuations?

Response: In this case, measurements were collected as frequently as possible; however the main goal was to track larger period fluctuations or seasonal changes in the environment. Given the larger spatial scale of the resistivity measurement and interpretation of early results we knew that measurable contrasts were most likely to occur through seasonal transitions. We did attempt to capture short-period transience, particularly during the second half of the study, which can be seen in the denser sampling interval in Figure 4.

Although we discuss the limitations of this study (data aliasing) and potential sources of thermal influence on the geophysical measurements, we do not neglect temperature fluctuations. These are considered to be an important component of the observed geophysical dynamics. Our sampling frequency considers longer-period (seasonal) variations rather than diurnal variations. Given this coarser sampling interval we cannot comment on the impacts of shorter-period diurnal temperature fluctuations. That being said, we did acknowledge the potential impact of sunlight (heating) of the riverbed and its spatial/temporal variability on the geophysical signatures, and thus, the timing of the measurement. We have enhanced this discussion with additional text and references (i.e., Constantz et al. 1994; Constantz 1998) on Lines 986-1012.

Line 262: “manually filtered” What criteria was used for manually filtering? Why was this approach used rather than the common quantitative method of envelope filtering based on an error model?

Response: In our case, only obvious data outliers were removed (e.g., failed measurements based on a non-zero standard deviation); we intentionally did not apply any pre-inversion data smoothing or

averaging in an attempt to preserve the data trends and maintain data-input consistency. However, data smoothing was directly applied in the inverse routine as described in the text. The approach used in any study will depend on the site conditions and desired outcome of the experiment. In our case, we were concerned with preserving the signal of the natural system (governed by multiple factors) rather than enhancing a particular element or physical processes in the model.

Measurement error is indeed a very important factor in the interpretation of resistivity data. Noise can arise from low signal (S/N ratio) such as electrode contact or instrumentation capabilities. These sources of noise are dynamic and minimized through data stacking in the field. Alternative sources of noise can arise from localized heterogeneities or non-uniform ground coupling, effectively resulting in the creation of artifacts in the data (2D solution to a 3D problem). Our filtering approach removed stacked measurements with a standard deviation exceeding a couple %; in most cases these data points were easily identified based a sudden/localized fluctuation in resistivity. However, the other and likely more significant source of error, arising from spatial heterogeneity, was not easily quantified due to our intentional use of a Wenner array. Although this array yields a higher S/N ratio it does not permit the collection of reciprocal data. Slater et al. 2000, *Journal of Applied Geophysics*, 44(2): 85-102, effectively quantifies this error as $e = R_n - R_r$, where the data noise, e , is determined from the normal and reciprocal resistivity measurement, R_n and R_r , respectively. Reciprocal data could have been collected in this study if we had used a dipole-dipole array; however, we found that the measured potentials (signal) associated with the dipole-dipole array were too low at the site (specifically at the pool), so these data sets were abandoned early on in the study.

We have incorporated a comment regarding our limited evaluation of measurement errors (given our choice of measurement array) and cited the work by Slater et al. (2000) on Lines 701-702.

Line 264: “moderate to high damping” – Does this mean different damping factors were used on each dataset? What is the numerical value of damping used and how is this value incorporated into your inversion scheme?

Response: We have revised the text to better reflect our approach Lines 637-648. Moderate dampening was used at the riffle while slightly higher-dampening was applied at the pool. Essentially, the dampening factors are used to reduce the likelihood of non-realistic model parameters through the inversion. This is applied in Res2DInv via the Marquardt-Levenberg modification to the Gauss-Newton equation given by $(\mathbf{J}^T \mathbf{J} + \lambda \mathbf{I}) \Delta \mathbf{q}_k = \mathbf{J}^T \mathbf{g}$, where \mathbf{J} is the Jacobian matrix, $\Delta \mathbf{q}$ is the model parameter change vector, \mathbf{g} is the discrepancy vector between measured and modeled data, and λ is the applied dampening factor, ranging from 0.01-1. We found that model solutions were at time converging toward unrealistic resistivities especially during the winter periods. Here, dampening factors of 0.2 and 0.3 for the riffle and pool effectively constrained the range of values of the components of the parameter change vector. Further explanation on this can be found in Loke (2002). We have added a supporting reference in the text on Line 645.

Line 267: What parameters, how were they optimized, and were identical settings used for all datasets?

Response: Our approach was effectively trial by error as is the case of most geophysical inversions. As described in the text, parameters were adjusted in an attempt to reduce the RMS error while maintaining realistic model parameters (i.e., resistivity range). We have revised the text between Lines 637-648 to clarify our approach.

Line 268 – 269: Certainly achieving the lowest possible RMS is not the optimal approach to achieve the most “believable” geophysical result. How does the RMS relate to observed measurement noise/errors? At what point is the inversion fitting noise?

Response: Minimizing the RMS error was done while monitoring the effective range in model resistivity. As we described above we did not collect the data necessary to generate a useful measurement error model based on reciprocal data, therefore, we cannot compare the magnitude of the model RMS relative to a data error model. We acknowledge that this may be a limitation of our study.

Line 280: Is there a reference for this Resistivity Index? What is the justification for manipulating the data in this way?

Response: The resistivity index (a broadly and routinely used normalization technique) was used here so that we could compare the transience observed between the pool and riffle sections relative to a standard datum. One of the reasons for doing this was to remove the biases of varying model range between the pool and riffle. The index simply allowed us to normalize the data sets to their mean value, permitting easier comparison of the timing and magnitude of transient events at each location. We do not believe that this requires a citation since the equation was developed based on the data collection style. We revised the text to better explain the use of this equation (Lines 649-652).

Line 293 – 294: Where is the data demonstrating upward head shown?

Response: This data was not presented and was based on data points not shown in Figure 2. Based on the points monitored in this study within the river (RSG4) and behind the liner (SCV6) the regional groundwater gradients are actually downward, although we do not believe this to be reflective of conditions proximal to the streambed (based on associated datasets). That being said, we have revised the text to reflect the data points that were monitored. These changes are shown between Lines 710-711.

Line 307/Figure 6b: It would be helpful to grade the colors of the lines linearly to more easily show the temperature trend. Even better would be to present these data as a matrix/grid where time is on the x-axis, depth is on the y-axis, and color represents temperature.

Response: We believe the current presentation of the data is reasonable as it is more easily interpreted. The purpose of the figure was to show the temperature dynamics with respect to depth, and the extent of the heterothermic zone, and illustrate the temporal variability overserved during the winter months. We think the current figure layout achieves these objectives.

Line 308: “correspond to areas” I cannot tell from the figure how the fracture patterns correspond to the temperature results. Perhaps some annotation, or another approach to presenting these data would help.

Response: In this case fractures are readily evident along the profile and the deviations in temperature are abundant. There is no singular feature or package of fractures, but rather varying degrees of variability due changing fracture density. This figure conveys the fracture density of sedimentary rock, showing both horizontal and vertical fractures, and sensitivity of the temperature profile in relation to the fracture distribution. This is meant to be first-order view of the fractures and thermal variability beneath the riverbed, so no additional annotation have been added.

Line 321 – 331: [Figure 8] This seems more like a discussion point rather than a result.

Response: In some ways this can be viewed as a point of discussion based on measured data; however, we felt that is was best placed prior to the introduction of the resistivity profiles. The figure is based on the results of Figure 5 and 6. We have revised the text (Lines 737-769) and the caption (Lines 1576-1583). We believe the current placement of this information is reasonable.

Line 356 – 358: “greater number of measurements. . .” why would the number of removed data cause higher RMS? Presumably if the data were removed, they would no longer be included in the RMS calculation.

Response: We have revised the text between Lines 795-846 to clarify this point. Essentially, more data points were removed during noisy periods. While bad (failed) measurements were removed, the overall dataset remained noisy overall, thereby resulting in higher RMS errors.

Line 374: What are the observed thicknesses of basal ice and floating ice?

Response: Unfortunately we were not able to measure the thickness of basal ice, but it was visually observed in the field. We have revised the text throughout to clarify this point.

Line 415-416: “groundwater discharge in this section” I don’t follow the logic why the relationship between substrate resistivity and “surface water response” indicates magnitude of discharge that could be interpreted in this way. Also, correlation is not demonstrated or quantified.

Response: We have revised the text to simply state that groundwater-surface water mixing either does not occur or that discharge is strong, thereby limiting potential mixing (Lines 917-920). The word correlation has been removed.

Line 432: “strong upward hydraulic gradients” please indicate where this is demonstrated by data.

Response: We have revised/reduced our emphasis of strong upward gradients in light of the reviewer comments above. We recognize that this was conjecture.

Line 436: “likely dominated the bulk electrical response” Why ‘likely’? Based on the evidence shown, temp is clearly dominating the ERT signal.

Response: We have now emphasized the importance of temperature on the resistivity signal and removed the word “likely” on Line 965.

Line 445: Where is ground frost or riverbed ice formation measured data shown?

Response: Neither ground frost or river bed ice were explicitly measured in this study. Ground frost was interpreted based on the resistivity data (Figure 11e), while riverbed ice (basal ice) was observed in the field as described in the text.

Line 459 – 473: As previously stated, data showing the frost and ice should be shown.

Response: Please see response above.

Line 474: I’m not sure what evidence directly supports this statement. The provided sensitivity analysis appears to only vary the river water electrical properties; this doesn’t seem to directly simulate the presence of ice as claimed in this statement.

Response: We’ve revised the text on Lines 1029-1040 to address this concern.

Line 479 – 480: Quantify this? Why would inputting a one-half of true river water resistivity lead to “substantial overestimates of river resistivity” – wouldn’t the river water resistivity be fixed so that the output = the input?

Response: We were referring to the bedrock resistivity. The surface water resistivity was fixed as stated. We have revised the text on Lines 1029-1040.

Line 486: What about a synthetic model example?

Response: At this point we have limited our results and discussion to the field measurements. A synthetic study would be very informative and could be considered in future work but would require additional borehole information to build a realistic physical model of the fractured bedrock.

Line 510: How does geoelectrical transience translate into hydrological processes?

Response: Changes in electrical resistivity across a fixed area over time are the result of variations in the electrical properties of the pore water. Changes can occur from temperature, specific conductance, or saturation (phase transformation such as ice formation). Surface water and groundwater typically exhibit distinct electrical properties as we show Figure 7. Whether these property variations can be exploited in a bedrock environment using surface geophysical methods has not previously been explored. Our study aims to assess the utility of surface geophysics, while also examining the utility of temperature and EC fluctuations to infer hydrological processes (e.g., thermal conduction, groundwater-surface water exchange, and fracture connectivity) in a bedrock river of varying morphologic conditions. There is an extensive body of literature demonstrating the use of temperature as a tracer for groundwater flux or flow across a riverbed. Here, we explore the sensitivity of surface electrical methods to seasonal temperature transience in the bedrock. This study does not address all elements of the conceptual model, but rather, represents a step toward a robust understanding.

Line 511 – 452: The conclusions section contains substantial summary and could be reworked for improved focus.

Response: The conclusions have been re-written to better highlight the specific contributions of our study and the implications to future work.

Figure 5: The purpose of this figure is unclear and I suggest that it could be deleted. The A/B/C/D locations are already indicated on Figure 12; the river stage information is presented on Figure 4; the location of the model block midpoints does not appear to be substantially important to the manuscript.

Response: Figure 5 has been removed.

Figure 9: Perhaps showing only the difference between these two maps would make interpretation easier? If not only difference, then perhaps just adding a third difference panel. Also, isocontour labels are too small to read.

Response: The revised Figure 8 now includes a % change plot between low and high stage periods, and the isocontours in these plots have been removed for clarity.

Figure 10: What is the model error relative to the measurement errors? What is the purpose of showing these vast bulk averages when that eliminates any of the valuable spatial information yielded by using tomographic methods? Figure 12 seems to be much more useful than this.

Response: The value of Figure 9 is that it documents the full time-series of the resistivity measurements at each location in the river and shows the range in values observed through the seasonal transitions. It also provides information about the ground conditions which have implications to the interpretation of

information in the subsequent figures. The vastly different resistivity conditions and their seasonal behavior is more clearly presented in Figure 9, than that (achievable) in Figure 10 or 11. It is also not possible to present all of the data in Figure 10 (2D sections), yet is important that the reader has an appreciation for the temporal position of these snapshots; in other works Figure 9 provides an important point of reference. Figure 9 also provides an overview of the data quality (e.g., data points removed and model RMS error) and the timing of those events. We believe this provides critical context for the transience presented in Figure 11.

It is reasonable to assume that the model RMS error is a representation of the measurement error. However, the source of the error remains unknown. Unfortunately, the nature of the measurement error cannot be examined in this study due to our choice of resistivity array geometry (Wenner vs. dipole-dipole). We believe the Wenner array was the best choice given the site conditions, and thus, are confident in our methodology given what we knew at the time. We believe that future work should consider the source of measurement errors, and the impacts these have on the model.

At this point we are confident that Figure 9 provides important and useful information for understanding the subsequent information of Figure 10 and 11.

Figure 11: Very nice layout and presentation of this figure, however certainly this needs to be replotted to show the difference between (b) through (h) relative to (a) in both columns

Response: Converting resistivity to relative % change was considered for Figure 10, but we believe it is best to maintain the absolute resistivity in this situation for two reasons: 1) the reader will be able compare the actual resistivity between the pool and riffle sections over the seasonal period, and 2) it maintains the structural distribution of the resistivity that would otherwise be lost or de-emphasized. We do evaluate the relative % change in resistivity using a Resistivity Index calculation in Figure 11.

References:

Loke M.H.: Tutorial: 2-D and 3-D electrical imaging surveys, Geotomo Software, Malaysia, 2002.

McNeill, J. D.: Electromagnetic terrain conductivity measurement at low induction numbers, Geonics Ltd. Technical Note, TN-6, 1980.

Van Dam, R.L., B.P. Eustice, D.W. Hyndman, W.W. Wood and C.T. Simmons: Electrical imaging and fluid modeling of convective fingering in a shallow water-table aquifer, Water Resources Research, 50, doi: 10.1002/2013WR013673.

Electrical Resistivity Dynamics beneath a Fractured Sedimentary Bedrock Riverbed in Response to Temperature and Groundwater/Surface Water Exchange

Colby M. Steelman¹, Celia S. Kennedy¹, Donovan Capes¹, Beth L. Parker¹

¹G360 Institute for Groundwater Research, College of Physical and Engineering Sciences, University of Guelph, Guelph, Ontario Canada

Correspondence to: Colby M. Steelman (csteelma@uoguelph.ca)

1 **Abstract.** Bedrock rivers occur where surface water flows along an exposed rock surface. Fractured sedimentary
2 bedrock can exhibit variable groundwater residence times, anisotropic flow paths, heterogeneity, along with
3 diffusive exchange between fractures and rock matrix. These properties of the rock will affect thermal transients in
4 the riverbed and groundwater-surface water exchange. In this study, surface electrical methods were used as a non-
5 invasive technique to assess the scale and temporal variability of riverbed temperature and groundwater-surface
6 water interaction beneath a sedimentary bedrock riverbed. Conditions were monitored on a semi-daily to semi-
7 weekly interval over a full annual period that included a seasonal freeze-thaw cycle. Surface electromagnetic
8 induction (EMI) and electrical resistivity tomography (ERT) methods captured conditions beneath the riverbed
9 along a pool-riffle sequence of the Eramosa River, in Canada. Geophysical datasets were accompanied by
10 continuous measurements of aqueous specific conductance, temperature and river stage. Time-lapse vertical
11 temperature profiling within a lined borehole adjacent to the river revealed active groundwater flow zones along
12 fracture networks within the upper 10 m of rock. EMI measurements collected during cooler high-flow and warmer
13 low-flow periods identified a spatiotemporal riverbed response that was largely dependent upon riverbed
14 morphology and seasonal groundwater temperature. Time-lapse ERT profiles across the pool and riffle sequence
15 identified seasonal transients within the upper 2 m and 3 m of rock, respectively, with spatial variations controlled
16 by riverbed morphology (pool verses riffle) and dominant surficial rock properties (competent verses weathered
17 rock rubble surface). While the pool and riffle both exhibited a dynamic resistivity through seasonal cooling and
18 warming cycles, conditions beneath the pool were more variable largely due to the formation of river ice during the
19 winter season. We show that surface electrical resistivity methods have the capacity to detect and resolve electrical
20 resistivity transience beneath a fractured bedrock riverbed in response to porewater temperature and specific
21 conductance fluctuations over a complete annual cycle.

Deleted: exchange

Deleted: imaging

Deleted: within

Deleted: , Guelph, Ontario

Deleted: ,

Deleted: V

Deleted: profiling

Deleted: conducted

Deleted: n

Deleted: inclined

Deleted: underlying

Deleted: through

Deleted: Resistivity

Deleted: conditions

Deleted: resistivity

Deleted: collected

Deleted: dynamic

Deleted: Although seasonal resistivity trends beneath the riverbed suggest groundwater discharge may be influencing the spatiotemporal extent of a groundwater-surface water mixing zone, intraseasonal resistivity transience suggest potential groundwater-surface water exchange across the upper few meters of rock

49 **1 Introduction**

50 Fractured sedimentary bedrock represents an important source of water for many communities around the world.
51 Although the effective porosity of rock is low relative to unconsolidated sediment, the existence of dense networks
52 of interconnected fractures, dissolution-enhanced conduits, and karst features, can result in productive yet
53 heterogeneous and anisotropic flow systems. An exposed bedrock surface may exhibit greater variability in flow
54 and transport properties as it is subjected to weathering and erosional processes, leading to very complicated
55 groundwater recharge and discharge patterns. Fractured sedimentary rock is best conceptualized as a dual porosity
56 system where fractures dominate flow, but remain connected to water stored in the porous matrix through advection
57 and diffusion. Such conceptualizations of fracture flow and transport are routinely applied to groundwater resource
58 (e.g., Novakowski and Lapcevic, 1998; Lemieux et al., 2009; Perrin et al., 2011) and contaminant transport studies
59 (e.g., Zanini et al., 2000; Meyer et al., 2008; McLaren et al., 2012). Recent studies have extended these concepts to
60 fluvial river environments (e.g., Singha et al., 2008; Toran et al., 2013a).
61 Groundwater-surface water interactions at the reach-scale are conceptualized through gaining, losing and flow-
62 through interactions (Woessner, 2000). At the channel scale, micro-to-macro bedform variations result in variably-
63 scaled zones of surface water downwelling (recharge) and groundwater upwelling (discharge) (e.g., Binley et al.,
64 2013; Käser et al., 2013). Groundwater temperature measurements are frequently used to monitor spatiotemporal
65 variations in groundwater-surface water exchange or flux across riverbeds (e.g., Anderson, 2005; Irvine et al., 2016).
66 Yet, very little is known about the existence and nature of hyporheic and groundwater-surface water mixing zones in
67 fractured sedimentary bedrock, largely because these systems are very difficult to instrument using direct methods
68 (e.g., drive point monitoring wells, seepage meters, thermistors) and the scale of the interaction may be very small
69 or heterogeneous relative to unconsolidated sediment.

70 Hydrologic processes along a fractured bedrock river were explored by Oxtobee and Novakowski (2002), who
71 concluded that groundwater-surface water interaction was restricted by poor vertical connectivity and limited
72 exposure of horizontal bedding plane fractures. A subsequent numerical sensitivity analysis by Oxtobee and
73 Novakowski (2003) confirmed that groundwater-surface water connectivity through discrete fractures would be
74 highly variable in space and time, and would largely depend on fracture size or aperture, river stage, and the
75 distribution of hydraulic head within the flow system. Fan et al. (2007) numerically explored the influence of
76 larger-scale fracture orientations and geometries on the groundwater flow system near a stream: they concluded that
77 the base flow to a stream would be higher for streams aligned with fracture dip than those aligned with fracture
78 strike. Therefore, groundwater-surface water interaction in a fractured bedrock environment will depend on stream-
79 fracture alignment. Although these previous studies offered valuable insights into the magnitude of groundwater-
80 surface water exchange, they were based on idealized fracture network conceptualizations, and did not consider the
81 role of matrix porosity and potential exchanges between fractures and the porous matrix.

82 Electrical and electromagnetic methods such as ground-penetrating radar, electromagnetic induction and electrical
83 resistivity imaging are commonly used to characterize fluvial deposits (e.g., Naegeli et al., 1996; Gourry et al., 2003;
84 Froese et al., 2005; Sambuelli et al., 2007; Rucker et al., 2011; Orlando, 2013; Doro et al., 2013; Crosbie et al.,

Deleted: . This can

Deleted: particularly in areas hosting dynamic interactions between groundwater and surface water

Deleted: may be

Deleted: While a number of

Deleted: r

Deleted: some of

Deleted: depositional

Deleted: ,

Deleted: there remain gaps in our conceptual understanding of groundwater-surface water interaction and exchange mechanisms in bedrock rivers where discrete fracture networks will dominate groundwater-surface water flux with secondary interactions supported by the porous rock matrix.

Deleted: ¶

Deleted: zones

Deleted: zones

Deleted: routinely

Deleted: evaluate

Deleted: equivalent processes in

Deleted: bedrock incision (i.e.,

Deleted:)

Moved (insertion) [3]

111 2014). The capacity of time-lapse electrical resistivity imaging for conceptualization of groundwater transients in
112 sediment is well-documented in the literature (e.g., Nyquist et al., 2008; Miller et al., 2008; Coscia et al., 2011;
113 Cardenas and Markowski, 2011; Musgrave and Binley, 2011; Coscia et al., 2012; Dimova et al., 2012; Wallin et al.,
114 2013). Electrical imaging of natural river systems perturbed by solute tracers has resulted in unprecedented
115 visualizations of fluid flow (e.g., Ward et al., 2010a, 2010b; Doetsch et al., 2012; Ward et al., 2012; Toran et al.,
116 2013a; Toran et al., 2013b; Harrington et al., 2014). More recent applications of electrical resistivity in karst
117 undergoing surface water transients have shown how surface geophysics can unravel complex hydrologic processes
118 in sedimentary bedrock environments (e.g., Meyerhoff et al., 2012; Meyerhoff et al., 2014; Sirieix et al., 2014),
119 especially when site conditions limit the use of more invasive direct measurement methods.

Deleted: also

120 While a variety of geophysical tools and techniques can measure flow and water chemistry in space and time
121 (Singha et al., 2015), the most appropriate tool and approach will depend on the scale of interest. The vast majority
122 of geophysical work within shallow river environments has utilized discrete temperature monitoring below the
123 riverbed to detect vertical fluxes (e.g., White et al., 1987; Silliman and Booth, 1993; Evans et al., 1995; Alexander
124 and Caissie, 2003; Conant, 2004; Anderson, 2005; Hatch et al., 2006; Keery et al., 2007; Schmidt et al. 2007;
125 Constantz, 2008). Recent advancements in distributed fiber optic cables have improved spatial and temporal
126 resolution of groundwater-surface water interactions (e.g., Slater et al., 2010; Briggs et al., 2012; Johnson et al.,
127 2012).

Deleted: assess

Deleted: ; these works have focused on processes within alluvial sediments

128 Groundwater and surface water interaction can be monitored through changes in thermal gradient or electrolytic
129 concentration (e.g., Norman and Cardenas, 2014), yet the scale and magnitude of these interactions will vary as a
130 function of riverbed architecture and subsurface hydraulic conditions (Crook et al., 2008; Boano et al., 2008; Ward
131 et al., 2012; Tinkler and Wohl, 1998) resulting in spatially dynamic exchange. These processes are further
132 complicated by diel (e.g., Swanson and Cardenas, 2010) and seasonal (e.g., Musgrave and Binley, 2011)
133 temperature fluctuations across a range of spatial scales, local transients such as precipitation events (e.g.,
134 Meyerhoff et al., 2012), river stage fluctuations (e.g., Bianchin et al., 2011) and controlled dam releases (e.g.,
135 Cardenas and Markowski, 2011). Relative to other non-invasive geophysical methods, electrical resistivity methods
136 are more robust in their ability to provide information about temperature and solute fluctuations beneath actively
137 flowing surface water bodies (e.g., Nyquist et al., 2008; Cardenas and Markowski, 2011; Ward et al., 2012;
138 Meyerhoff et al., 2014) particularly in a time-lapse manner. Unlike conventional hydrogeological methods (e.g.,
139 screened or open coreholes), which may bias conduction in the fractures, surface electrical methods are sensitive to
140 the bulk electrical conductivity of the formation, making them more suited for detection of processes between the
141 open fractures/conduits and the porous matrix.

Deleted:

Deleted: Fractured sedimentary bedrock exhibits complex flow systems, where the bulk of the flow the fracture network, with highly-variable head distributions; matrix storage may support equally complex biogeochemical processes and thermal dynamics through convective or diffusive exchange with open fractures or dissolution-enhanced features (Fig. 1).

Moved down [1]: Ward et al. (2010a) demonstrated how surface electrical methods can be used to detect and quantify diffusive mass transport (exchange) between a mobile and immobile storage zone in a shallow riverbed.

Deleted: Therefore, we hypothesize that

Deleted: a

Deleted: – encompassing fracture and matrix flow and diffusion –

Moved (insertion) [1]

Deleted: can

142 A hypothetical groundwater-surface water mixing zone in a porous fractured rock system (Fig. 1) will exhibit
143 transience in water temperature and specific conductance as a result of changes in groundwater flow (recharge vs.
144 discharge), mixing of surface water and groundwater, seasonal atmospheric temperature fluctuations and/or
145 biogeochemical changes within the riverbed. Ward et al. (2010a) demonstrated how surface electrical methods
146 sensitive to changes in water conductivity could be used to detect and quantify diffusive mass transport (exchange)

172 between a mobile and immobile storage zone in a shallow riverbed. Our study uses a similar geophysical
 173 monitoring approach to assess the magnitude and scale of groundwater-surface water transience beneath a fractured
 174 bedrock riverbed based on the detection and characterization of geoelectrical dynamics over a complete annual
 175 cycle. Seasonal freezing and thawing of surface water bodies is an important process in mid-latitude climates;
 176 winter freeze-up will reduce base flow contributions, while spring snow melt will result in a sudden and large
 177 increase in base flow to a river. Therefore, understanding the transient behaviours of the hydrogeologic system,
 178 including water-phase transformations, over a complete annual cycle will be critical to our understanding of the
 179 magnitude and spatial extent of groundwater-surface water exchange along fractured bedrock rivers. Given the
 180 challenges and costs associated with installing sensors within rock and heterogeneous flow system characteristics,
 181 minimally invasive surface and borehole geophysical methods offer an ideal alternative, and possibly, more
 182 effective approach for long-term groundwater-surface water monitoring of bedrock environments.

183 Our study examines the capacity of electrical imaging methods (i.e., electromagnetic induction and electrical
 184 resistivity) to monitor geoelectrical transients within a fractured sedimentary bedrock river to better understand
 185 groundwater-surface water transience over a complete annual cycle. To achieve this, seasonal variations in
 186 electrical resistivity distribution were measured across a 200 m reach of a bedrock river using a ground conductivity
 187 meter and time-lapse electrical resistivity measurements along two fixed transects intersecting a pool-riffle
 188 sequence. These geophysical surveys were supported by continuous measurements of groundwater and surface
 189 water temperature, specific conductance and river stage. Our study shows that spatiotemporal resistivity dynamics
 190 were largely controlled by riverbed morphology in combination with seasonal changes in water temperature, and to
 191 a lesser-degree electrolytic concentration. The formation of ground frost and basal ice strongly affected the
 192 electrical resistivity beneath the riverbed compared to intraseasonal dynamics (spring, summer and fall). Observed
 193 geoelectrical changes beneath the riverbed appear primarily dependant on seasonal temperature trends exhibiting
 194 varying zones of influence (vertical and horizontal) across the pool and riffle section of the river. The riverbed was
 195 strongly susceptibility to seasonal atmospheric temperature fluctuations, which might have implications to
 196 biogeochemical processes or benthic activity.

197 **2. Background**

198 The Eramosa River – a major tributary of the Speed River within the Grand River Watershed in Ontario, Canada –
 199 resides upon a regional bedrock aquifer of densely fractured dolostone with dissolution-enhanced conduits and karst
 200 features (e.g., Kunert et al., 1998; Kunert and Coniglio, 2002; Cole et al., 2009). Although this aquifer represents
 201 the sole source of drinking water for the region, the potential effects of increased groundwater pumping on the
 202 overlying bedrock river and surrounding ecosystems, are not yet understood. This is largely due to a gap in our
 203 conceptual understanding of groundwater-surface water interaction in rivers that flow directly along sedimentary
 204 bedrock surfaces with exposed fracture networks. The fractured sedimentary bedrock exhibits a complex flow
 205 system due to variably connected fracture networks, dissolution-enhanced features, and variable bedrock exposure
 206 (Steelman et al. 2015a, 2015b). The bulk of the flow will occur along the fracture networks, with highly-variable

Deleted: may be identified within a fractured bedrock riverbed by monitoring spatiotemporal changes groundwater temperature and porewater electrical conductivity using minimally invasive electrical resistivity methods. The detection of seasonal transients beneath the bedrock riverbed would support future conceptualizations of groundwater-surface exchange along fractured bedrock rivers.

Deleted: Our

Deleted: focuses on

Deleted: along

Deleted: the Eramosa River in Ontario, Canada

Deleted: .

Deleted: S

Deleted: . Based on c

Deleted: .

Deleted: s

Deleted: Over a complete annual cycle,

Deleted: during the winter season was accompanied

Deleted: by stronger geoelectrical

Deleted: than intraseasonal

Deleted: transience in the flow system

Deleted: These geoelectrical observations support the existence of a predominant groundwater discharge zone with limited groundwater-surface water mixing

Deleted: .

Deleted: Background¶
 2.1 Geophysical Investigations along Streams and Rivers ¶

Moved up [3]: Electrical and electromagnetic methods such as ground-penetrating radar, electromagnetic induction and electrical resistivity imaging are commonly used to characterize fluvial deposits (e.g., Naegeli et al., 1996; Gourry et al., 2003; Froese et al., 2005; Sambuelli et al., 2007; Rucker et al., 2011; Orlando, 2013; Doro et al., 2013; Crosbie et al., 2014). The capacity of time-lapse electrical resistivity imaging for conceptualization of groundwater transients in sediment is also documented in the literature (e.g., Nyquist et al., 2008; Miller et al., 2008; Coscia et al., 2011; Cardenas and Markowski, 2011; Musgrave and Binley, 2011; Coscia et al., 2012; ...)

Moved down [4]: 2.2 Electrical Properties of the Subsurface¶ ...

Deleted: 2.3 Field Site Description

Moved (insertion) [5]

428 head distributions; matrix storage could support equally complex biogeochemical processes and thermal dynamics
429 through convective or diffusive exchange with open fractures or dissolution-enhanced features.

430 A focused geophysical investigation was carried out along a 200 m reach of the Eramosa River (Fig. 2). The study
431 area was positioned at a bend in the river with relatively cleared vegetation along the south shoreline and adjacent
432 floodplain with exposed rock at surface. A network of coreholes (continuously cored boreholes) and streambed
433 piezometers were installed across the site. Locally, the water table elevation corresponds to the surface water or
434 stage elevation, resulting in vadose zone thicknesses from <0.5 m to 2.0 m along the shorelines. The temperate
435 southern Ontario climate subjects the river to a wide-range of seasonal conditions, including high precipitation
436 periods in spring and fall, hot and dry summers, and variable degrees of ground frost and surface water freeze-up
437 during the winter months (Fig. 3a).

438 Locally, the river incises the Eramosa Formation by 2 m to 3 m exposing abundant vertical and horizontal fractures
439 with little to no alluvial sediment deposited along the riverbed (Fig. 3b). Regionally the Eramosa acts as a
440 discontinuous aquitard unit (Cole et al. 2009); however, core logs collected at the study site show bedding plane and
441 vertical joint set fractures spanning the entire 11 m sequence of Eramosa. This upper formation is underlain by
442 approximately 3 m of cherty, marble-like Goat Island formation, which exhibits high-angle fractures along cherty
443 nodules near the Eramosa contact. The Goat Island is underlain by more than 15 m of Gasport formation, which
444 exhibits coral reef mounds of variable morphology. The rock matrix of the Gasport is visually more porous with
445 well-defined vugs, dissolution-enhanced features, and fewer fractures than the overlying Goat Island and Eramosa.
446 A full-description of these bedrock sequences can be found in Brunton (2009).

447 In this region, the winter season may be accompanied by the formation of ground frost and surface water freezing.
448 Seasonal freeze-up will consist of an ice crust layer on the surface of the water and the possible formation of basal
449 ice along the riverbed (Stickler and Alfredsen, 2009). The latter phenomenon can occur during extreme atmospheric
450 cooling over turbulent water bodies, resulting in super-cooled water (<0°C) that rapidly crystallizes to form frazil
451 (i.e., tiny ice particles with adhesive characteristics); these crystals can flocculate to form slush, which adheres and
452 accumulates on the substrate forming a basal ice layer.

453 3 Methods

454 3.1 Electrical Properties

455 Electrical resistivity methods are based upon Ohm's Law ($R = \Delta V/I$). In the case of a homogeneous half-space,
456 the electrical resistance (R) of the subsurface is determined by measuring the potential difference (ΔV) across a pair
457 of 'potential' electrodes due to an applied current (I) across a pair of 'current' electrodes some distance away. The
458 measured R (Ω) across a unit volume of the earth can be converted to apparent resistivity (Ω m) using a specific
459 geometric factor that compensates for varying electrode array geometry (Reynolds, 2012). Apparent resistivity
460 measurements are commonly interpreted using tomographic inversion techniques, whereby measured data is
461 reconstructed from forward models of an optimized physical parameter distribution (Snieder and Trampert, 1999;
462 Loke et al., 2013). Although data inversion techniques are standard practice in the interpretation of most

Moved up [5]: (e.g., Kunert et al., 1998; Kunert and Coniglio, 2002; Cole et al., 2009)

Deleted: The Eramosa River is a major tributary of the Speed River within the Grand River Watershed, Ontario, Canada, and resides upon a bedrock aquifer of densely fractured dolostone of Silurian age with dissolution-enhanced conduits and karst features (e.g., Kunert et al., 1998; Kunert and Coniglio, 2002; Cole et al., 2009). Outcrops, core logs and geophysical data collected along the Eramosa River (e.g., Steelman et al., 2015a; Steelman et al., 2015b) indicate abundant vertical and horizontal fracture networks and karst features intersecting and underling the river. These field observations support the existence of a potential groundwater-surface water mixing controlled by discrete fracture networks and dissolution-enhanced features. ¶

Deleted: between

Deleted:

Deleted:

Deleted: formation

Deleted: variable

Deleted: This

Moved (insertion) [4]

Deleted: 2

Deleted: 2

Deleted: of the Subsurface

495 geophysical data, the model that best matches the measured data is not necessarily an exact representation of the
496 subsurface. Here, the inversion process ultimately yields a smoothed representation of the true parameter
497 distribution.

Deleted: T

Deleted: actual

498 The bulk electrical resistivity (i.e., inverse of conductivity) of a fluid-saturated medium can be calculated through a
499 simple empirical relationship known as Archie's Law (Archie, 1942):

Deleted: a

Deleted: formation

500
$$\rho_b = \phi^{-m} \rho_w, \quad (1)$$

501 where the resistivity of the bulk formation (ρ_b) is related to the porosity of the medium (ϕ) raised to the negative
502 power (m), which represents the degree of pore cementation, and the resistivity of the pore fluid (ρ_w) (Glover 2010).

Deleted: simply

503 This relationship carries a number of simplifying assumptions: the most significant being that the current flow is
504 entirely electrolytic. While more sophisticated formulations of Archie's Law incorporating fluid saturation and
505 interfacial conduction can be found in the literature (e.g., Rhoades et al., 1976; Waxman and Smits, 1968), Eq. (1) is
506 considered to be a reasonable approximation for this environment. Equation (1) is used in this study to evaluate the
507 impact of observed groundwater and surface water aqueous conductivity variations on the bulk formation resistivity.
508 Here, a value of 1.4 was used for the constant m , which is considered reasonable for fractured dolostone. It should
509 be noted that the relative impact of aqueous conductivity changes on the bulk formation resistivity may vary with
510 clay content and pore connectivity due to intrinsic deviations in the m value (Worthington, 1993). Furthermore,
511 orientated fracture networks may result in an anisotropic resistivity response (Steelman et al., 2015b); however,
512 these static properties of the rock will not impact relative changes in resistivity at a fixed location.

Deleted: in a saturated relatively clay-free

513 The electrolytic (fluid phase) resistivity will depend on the concentration and composition of dissolved ions, and
514 viscosity of the pore water (Knight and Endres, 2005). Increasing ion concentrations and temperature will lead to a
515 reduction in formation resistivity. Empirical evidence has shown that resistivity can decrease anywhere from 1 % to
516 2.5 % per °C (Campbell et al., 1948; Keller, 1989; Brassington, 1998). The effects of temperature on our resistivity
517 signals were determined using Arps's law (Arps, 1953):

Deleted: T

Deleted: corrections

Deleted: can be made

518
$$\rho_{w2} = \rho_{w1} \frac{(T_1 + 21.5)}{(T_2 + 21.5)}, \quad (2)$$

519 where ρ_w (Ω m) and T (°C) represent the resistivity and temperature of the water at two points. This formulation
520 was developed from a least-squares fit to the conductivity of a NaCl solution ranging from 0°C to 156°C; however,
521 the exact relationship between fluid conductivity and temperature will depend on the composition of the electrolytic
522 solution (Ellis, 1987).

523 **3.2 Bedrock Lithology, Fractures and Porosity**

Deleted: 1

524 The geology was characterized through a series of vertical and angled coreholes along the southern shoreline that
525 were advanced into upper Gasport formation. These drilling activities were part of a broader hydrogeological
526 investigation of groundwater flow and fluxes along the river. A network of riverbed piezometers, bedrock stage

538 gauges, and flux measurement devices were installed between 2013 and 2014 within the pool. Locally, the riverbed
539 morphology can be distinguished in terms of the amount of bedrock rubble or weathered rock fragments covering
540 the exposed rock surface. Figure 2 shows the transition from a rubble dominated riverbed (RDR) to a more
541 competent rock riverbed (CRR); this boundary roughly corresponds to the riffle-pool transition.

Deleted: blanketing

542 Geophysical measurements were supported by temperature, specific conductance of the fluid and river stage
543 elevation collected at nearby monitoring points (Fig. 2). The geologic and hydrogeologic data were obtained from a
544 river stage gauge (RSG4), a vertical corehole (SCV6) drilled to a depth of 10.9 m, and an angled corehole (SCA1)
545 drilled to a vertical depth of 31.8 m. The angled corehole plunges at 60° and is orientated at 340°, and therefore,
546 plunges beneath the river with a lateral displacement of 21 m. Coreholes were drilled using a small-diameter
547 portable Hydrocore Prospector™ drill with a diamond bit (NQ size: 47.6 mm core and 75.7 mm corehole diameter)
548 and completed with steel casings set into concrete to a depth of 0.6 m below ground surface (bgs). All coreholes
549 were sealed using a flexible impermeable liner filled with river water (FLUTE™ Flexible Liner Underground
550 Technologies, Alcalde, New Mexico, USA) (Keller et al., 2014).

Deleted: footprint spanning approximately

Deleted: from its surface expression

551 The SCA1 rock core was logged for changes in lithology, vugs, and fracture characteristics, intensity and
552 orientation, including bedding plane partings. Rock core subsamples were extracted for laboratory measurements of
553 matrix porosity using the following procedure: sample was oven dried at 40°C; dimensions and dry mass recorded;
554 samples evacuated in a sealed chamber and imbibed with deionized water; sample chamber pressurized to 200 psi to
555 300 psi for 15 minutes; samples blotted and weighed to obtain saturated mass. Open coreholes were logged using an
556 acoustic (QL40-ABI) and an optical (QL40-OBI) borehole imager (Advanced Logic Technologies, Redange,
557 Luxembourg), to characterize the fracture network.

558 **3.3. Pressure, Temperature, Specific Conductance and River Flow**

Deleted: 2

Deleted: Flux

559 Temperature, specific conductance and hydraulic pressure data were recorded using a CTD-Diver™ (Van Essen
560 Instruments, Kitchener, Canada) deployed within RSG4 (surface water) and SCV6 (groundwater) at a depth of 10.5
561 m bgs. The transducer in SCV6 was placed near the bottom of the open corehole prior to being sealed with an
562 impermeable liner, thereby creating a depth-discrete groundwater monitoring point. Surface water data were
563 recorded through the full study period while deeper bedrock conditions were recorded from early-September 2014
564 through late-May 2015. All measurements were collected at 15 minute intervals.

565 Vertical temperature profiles were additionally collected along the inclined sealed corehole water column of SCA1
566 from 4-Sep-2014 to 22-May-2015 using an RBRsolo™ temperature logger paired with a RBRsolo™ pressure logger
567 (RBR Limited, Ottawa, Canada). These data were recorded at 0.5 second intervals while the sensors were manually
568 lowered into the water column using a fiberglass measuring tape at a rate of 0.02 m s⁻¹ to 0.03 m s⁻¹. Barometric
569 pressure was collected at the site using a Baro-Diver™ (Van Essen Instruments, Kitchener, Canada). These
570 temperature sensors can resolve changes to 0.5×10⁻⁴ °C with a full-scale response time of 99 % in 2 seconds. ▼

Formatted: Superscript

Deleted: ¶

571 Rainfall was recorded at the University of Guelph Turfgrass Institute, located 2 km northwest of the site, while
572 snowfall accumulation was obtained from the Region of Waterloo Airport roughly 18 km south west of the site.

580 Hourly mean river flux was recorded 900 m upstream at the Watson Road gauge operated by the Grand River
581 Conservation Authority. A summary of the weather and river flux data are provided in Fig. 4.

582 3.4 Riverbed Electrical Resistivity

Deleted: 3

583 3.4.1 Spatial Electrical Resistivity Mapping

Deleted: 3

584 ~~Spatial~~ riverbed resistivity distribution was measured using a Geonics EM-31 ground conductivity meter (Geonics,
585 Mississauga, Canada) during a seasonally cool and warm period: ~~mid-summer/low-stage conditions on 7-Jul-2014~~
586 ~~and~~ early-spring/high-stage conditions on 3-Apr-2013. Measurements were collected at a rate of 3 readings per
587 second with the device operated in vertical dipole mode held ~1 m above the riverbed. The effective sensing depth
588 of this instrument in vertical dipole mode is approximately 6 m (~~cumulative depth~~), and is minimally sensitive to
589 conditions above the ground surface (McNeil, 1980). Data was recorded along roughly parallel lines spaced ~1.75
590 m apart orthogonal to the river orientation, with the coils aligned parallel to surface water flow direction. Water
591 depths over the investigated reach varied from <0.1 m in the riffle during low-flow to nearly 1 m in the pool during
592 high-flow conditions. Data sets were filtered for anomalous outliers prior to minimum curvature gridding.

Deleted: R

Deleted: electrical

Deleted: initially

Deleted: and mid-summer/low-stage conditions on 7-Jul-2014

593 3.4.2 Time-Lapse Electrical Resistivity Imaging

Deleted: 3

594 Surface electrical resistivity measurements were collected along two ~~fixed~~ transects orientated orthogonal to the
595 river (Fig. 2), capturing conditions within a pool and riffle sequence (Fig. 3). Line 1 was positioned downstream
596 over a deeper pool section with more substantial bedrock incision into a competent bedrock surface (Fig. 3b, i and
597 ii), while line 2 was situated upstream over a shallower riffle section blanketed by bedrock rubble fragments with less
598 bedrock incision (Fig. 3b, iii).

599 For this study, resistivity cables were constructed using a pair of 25 multicore cables (22 gauge strained wire, 600V
600 rating) wound within a PVC jacket. The PVC jacket was split open every meter to expose and cut out a single wire
601 that was connected to an audio-style banana plug. Spliced sections of outer PVC jacket were resealed using heat
602 shrink tubing and silicon. This process ~~yielded~~ two 24 channel cables each connected to a single multi-pin
603 connector for direct data logger communication. Electrodes were constructed from half-inch diameter stainless steel
604 rod cut to 6 inch lengths. A hole was drilled on one end of the electrode to receive the banana plug connector.
605 Given the exposed bedrock across the site, a half-inch hole was drilled into the rock at 1 m intervals along the
606 ground surface. In some cases, electrodes were buried beneath a rubble zone of the riverbed, or were pushed into a
607 thin layer of sediment. On the shorelines electrodes were fully implanted into the rock along with a few teaspoons
608 of bentonite clay to minimize contact resistance. Each monitoring line was instrumented with dedicated electrodes
609 and cables that remained in place for the duration of the study.

Deleted: resulted

Deleted: in

610 Resistivity measurements were recorded using a Syscal Junior Switch 48 (Iris Instruments, Orléans, France)
611 resistivity meter. A Wenner array was selected for its higher S/N ratio. A dipole-dipole array was tested, but found
612 to be very susceptible to noise (i.e., ~~bad data points~~ ~~resulting from~~ ~~low potentials~~); this ~~can be~~ attributed to the high-
613 contact resistances with rock combined with the instruments ~~more~~ moderate power capability (max 400 V, 1.3 A).

Deleted: excessive number of

Deleted: due

Deleted: to

Deleted: measured

Deleted: was

629 Although the Wenner array geometry resulted in a stronger signal (i.e., where potentials are measured across a pair
 630 of electrodes located between the current electrodes), it was less sensitive to lateral variations across the riverbed
 631 and did not permit the collection of a reciprocal dataset, which could have been used to assess potential
 632 measurement errors (e.g., Slater et al., 2000). Surface resistivity data were recorded on a semi-daily to semi-weekly
 633 interval from 18-Jul-2014 to 3-Jul-2015 covering a complete annual cycle, which included a seasonal freeze-thaw
 634 cycle, and numerous wetting-drying events accompanied by large river stage fluctuations. The timing of resistivity
 635 measurement events are shown along the river flow data in Fig. 4. Resistivity measurements were generally
 636 recorded between 8 AM and 1 PM.

637 Measured apparent resistivity data was manually filtered to remove erroneous data points prior to being inverted
 638 using RES2DINV v.3.59 (Geotomo Software, Malaysia), which uses the Gauss-Newton least-squares method (Loke
 639 and Dahlin, 2002). For this study, a robust inversion scheme was used with a moderate dampening factor applied at
 640 the riffle and a slightly higher dampening factor at the pool. These dampening factors were chosen based on the
 641 resistivity contrasts observed along the rock surface, along with intermittently noisy measurements at the pool; the
 642 width of the model cells were set to half the electrode spacing (i.e., model refinement) to help suppress the effects of
 643 large surface resistivity variations on the inversion process. All other parameters within the program were optimized
 644 to compensate for high noise and large resistivity contrasts, while achieving the lowest possible model root mean
 645 squared (RMS) error (Loke, 2002). Each model was independently inverted with a defined surface water boundary
 646 (i.e., stage height above the submerged electrodes) and true aqueous resistivity, both of which were fixed for each
 647 model inversion. The same set of initial inversion parameters was applied to all datasets collected along a given
 648 line. Model convergence typically occurred within 8 iterations.

649 Temporal variations in bedrock resistivity were assessed within 5 m wide × 2.5 m deep zones beneath the riverbed
 650 based on a resistivity index (RI) calculation. This enabled comparison of datasets with different magnitudes of
 651 resistivity variation. The RI was defined as follows:

$$652 \quad RI_{i,j} = \frac{MZR_{i,j} - MAR}{MAR}, \quad (3)$$

653 where $RI_{i,j}$ = resistivity index for the i^{th} zone on the j^{th} sample date; $MZR_{i,j}$ = mean zone resistivity for the i^{th} zone
 654 on the j^{th} sample date; MAR = mean annual resistivity of the entire profile across the full time series for the pool or
 655 riffle.

656 4 Results

657 4.1 Bedrock Fracture Network, Temperature and Specific Conductance

658 Formation contacts of the Eramosa–Goat Island and the Goat Island–Gaspport formations were identified in core at
 659 depths of 8.6 and 13.0 m bgs, respectively (Fig. 5a). Fractures beneath the river were predominantly horizontal to
 660 slightly dipping ($<10^\circ$), and most abundant in the Eramosa and Goat Island. Although vertical and sub-vertical
 661 fractures ($>10^\circ$) were relatively less abundant than bedding plane fractures, they were more uniformly distributed

Deleted: s

Deleted: with an equal inter-electrode spacing

Deleted: will

Deleted: be

Deleted: compared to the dipole-dipole array

Deleted: , and thus, less sensitive to the presence of a single or package of vertical fractures between adjacent electrodes

Deleted: with corresponding

Deleted: rates

Deleted: and atmospheric data

Deleted: to

Deleted: s given the high

Deleted: and

Deleted: datasets

Deleted: .

Deleted: T

Deleted: ¶
 Figure 5 shows the model setup for the pool and riffle, including the minimum and maximum river stage elevations observed during the geophysical monitoring events. A portion of the electrodes were variably submerged beneath a surface water layer. Stage elevations ranged from 310.92 masl to 311.32 masl at line 1, and 311.09 masl to 311.48 masl at line 2. Thus,

Deleted: e

Deleted:

Deleted: within four representative zones

Deleted: (A, B, C and D; Fig. 5) using

Deleted: a

Deleted: .

Deleted: These zones were chosen based on their contrasting bedrock conditions, relative position along the river transect and geophysical dynamics observed during the monitoring period. The

Deleted: was calculated

Deleted: for the pool and riffle resistivity profile

Deleted: Fig. 6

706 with depth. These high-angle fractures terminate at surface as vertical joint sets along two regional orientations: 10°
707 to 20° NNE and 280° to 290° SNW (Fig. 3b, ii). Matrix porosities from the corehole, ranged from 0.5 % to 5 %, with
708 the lowest porosities observed along the highly weathered riverbed surface and lower portion of the Eramosa
709 Formation. Hydraulic head data collected in the river and at the base of SCV6 (10.5 m bgs) suggest a seasonally
710 sustained downward gradient ranging from 0.21 to 0.26 at the pool, however, this does not necessarily reflect
711 conditions proximal to the streambed,
712 Vertical temperature profiling within the static water column of the FLUTE™ lined SCA1 corehole from 4-Sep-
713 2014 to 22-May-2015 captured seasonal fluctuations in ambient groundwater temperature to depths up to 20 m (Fig.
714 5b), thereby delineating the vertical extent of the heterothermic zone. Temperatures inside the liner ranged from
715 18°C in late-summer, to 5°C in mid-winter. Although fluctuations were observed along the entire 20 m profile, the
716 bulk of the variations (short and long-period) were observed in the upper 10 m bgs.

717 Previous studies using ambient temperature profiling in lined coreholes (Pehme et al. 2010; Pehme et al. 2014)
718 examined the effects of active groundwater flow around static water columns. Pehme et al. (2010) demonstrated
719 how a lined water-filled corehole in thermal disequilibrium with the surrounding formation would exhibit more
720 short-period temperature perturbations along its vertical profile than an equilibrated water column within zones of
721 active groundwater flow. Here, the onset of winter seasonal conditions (9-Jan-2015 through 31-Mar-2015) cooled
722 the corehole water column near the ground surface resulting in density-driven convection within the column, leading
723 to thermal disequilibrium with respect to the surrounding bedrock resulting in subtle temperature perturbations as
724 the water column cooled toward 5°C. The magnitude and frequency of the perturbations observed in Fig. 5b during
725 these cooler periods correspond to areas of increased fractures (Fig. 5a), supporting active groundwater flow,
726 Specific conductance and temperature of surface water (RSG4) and groundwater (SCV6) corresponding to
727 geophysical sampling events (Fig. 4) are presented in Fig. 6. These data indicate that surface water specific
728 conductivity varied within a much narrower range than the actual (uncompensated) conductivity, which includes the
729 effects of temperature. While the overall impact of temperature and ionic concentration on the specific conductance
730 of surface water were similar (i.e., equivalently dynamic), variations associated with ionic concentration appear
731 more erratic, exhibiting sharper fluctuations over shorter periods of time. For instance, major precipitation events
732 coinciding with measurement events 13, 26 and 31 (refer to Fig. 4) were accompanied by short-period reductions in
733 surface water conductivity and increases in temperature. Seasonal atmospheric temperature trends resulted in more
734 gradual, yet sustained reductions in aqueous conductivity. In comparison, the groundwater specific conductance at
735 10.5 m bgs was comparatively stable during the study period, exhibiting a moderate temperature driven decline
736 superimposed by shorter-period fluctuations associated with ion concentration.

737 Figure 7 shows the potential impact of these observed specific conductivity and temperature variations (based on
738 Fig. 5b and 6) on the bulk formation resistivity using Eq. (1) and Eq. (2) for three representative porosity values.
739 Porosities of 1 % and 5 % correspond to the values obtained in core, while a porosity of 35 % is assumed to
740 represent s the maximum porosity of a weathered or broken rubble zone (i.e., unconsolidated porous sediment).

Deleted: were relatively low, ranging

Deleted: .

Deleted: upward

Deleted: vertical

Deleted: (i.e., groundwater discharge zone)

Deleted: .

Deleted:

Deleted: Fig. 6

Deleted: abrupt

Deleted: Fig. 6

Deleted: frequency

Deleted: Fig. 6

Deleted: .

Deleted: indicating

Deleted: zones beneath the riverbed

Deleted: Fig. 7

Deleted: and exhibited

Deleted: seasonally

Deleted: Figure 8

Deleted: Fig. 6

Deleted: 7

Deleted: might

764 These calculations indicate that variations in temperature will likely be the primary driver in formation resistivity
 765 dynamics. For instance, water temperature could affect the formation resistivity by as much as 46 % (between
 766 isotherms), based on the observed range in groundwater and surface water temperatures, respectively. In
 767 comparison, measured aqueous conductivity ranges (along an isotherm) for groundwater and surface water would
 768 affect the formation resistivity by 18 % and 36 %, respectively. These maximum temperature effects represent end-
 769 member conditions for a given specific conductance and effective porosity estimate.

Deleted: particular
Deleted: specific
Deleted: y
Deleted: The natural system will exhibit a much more complex distribution of formation resistivity given variable fracture networks, matrix porosity, and dissolution-enhanced features.

770 **4.2 Sub-Riverbed Electrical Resistivity Distribution**

771 Two ground conductivity surveys were conducted across the riverbed surface to assess spatial variability in bulk
 772 formation resistivity and its relationship to riverbed morphology (e.g., pool vs. riffle): resistivity snapshots were
 773 collected on 7-Jul-2014 during low-flow conditions (1.30 m³ s⁻¹) and on 3-Apr-2013 during high-flow conditions
 774 (6.81 m³ s⁻¹) (Fig. 8a). The percentage change in resistivity from low to high-stage periods is shown in Fig. 8b. The
 775 daily average river flows for the years 2013 and 2014 were 3.5 m³ s⁻¹ and 3.3 m³ s⁻¹, respectively.

Deleted: the first
Deleted: was
Deleted: Fig. 9
Deleted: while the second was collected on 7-Jul-2014 during low-flow conditions (1.30 m³ s⁻¹) (Fig. 9b)

776 Two main observations can be made from the changes observed between warmer low-flow and cooler high-flow
 777 conditions. First, the southern shoreline exhibited a 10% to 15% reduction in resistivity along the southern shoreline
 778 within the pool and along the cut bank (outer edge of the elbow). These areas were characterized by more
 779 competent rock with exposed bedding plane fractures and vertical joint (Fig. 3b, i). Secondly, a broader and more
 780 variable increase in resistivity upwards of 20% to 25% was observed northward into the thalweg along the slip-off
 781 slope (inner edge of the elbow) and the eastern and western portions of the reach; the rock surfaces in these areas
 782 were more weathered with large irregular rock fragments and dissolution features, and limited exposure of
 783 horizontal bedding plane fractures. A lower resistivity zone (blue area) was identified upstream within the northern
 784 portion of the riffle section (Fig. 3b, iii). The riffle portion of the river was also accompanied by a break in the high
 785 resistivity trend observed along the south shoreline. A lower average resistivity was observed during warmer low-
 786 flow conditions indicating that a portion of the response may be dependent on formation temperature (i.e., 5°C to
 787 20°C fluctuations). However, the reduction in resistivity along the cut bank during cooler high-stage period indicates
 788 an increase in the specific conductance of the pore fluid, which would be consistent with increased baseflow and
 789 groundwater discharge to the river.

Deleted: and warmer low-flow
Deleted: the
Deleted: highest resistivity (red areas) with the least temporal variability
Deleted: are
Deleted: and less-fractured rock
Deleted:
Deleted: more dynamic
Deleted: response
Deleted: and
Deleted: north
Deleted: shoreline
Deleted: was

790 **4.3 Time-Lapse Electrical Resistivity Imaging**

791 **4.3.1 Electrical Resistivity Models**

792 Figure 9 provides a summary of the inverted model results at the pool (Fig. 9a) and riffle (Fig. 9b) sections for the
 793 full study period. The mean inverted model resistivity and data range for each sample event is presented along with
 794 the number of apparent resistivity data points removed from the dataset prior to inversion, and the root mean squared
 795 (RMS) error of the inverted model. The partially-frozen and frozen ground conditions were accompanied by higher
 796 signal noise due to a systematic increase in electrode contact resistance and reduction in pore fluid connectivity
 797 (liquid water saturation near the surface); here, lower potentials resulted in more frequent failed measurement, which
 798 had to be removed from the dataset prior to inversion. Therefore, the noisier datasets collected in these periods were

Deleted: with
Deleted: Formation resistivities varied up to 10 % within the pool and up to 18 % within the riffle. While the average change in riverbed resistivity was 16 %, portions of the riverbed further down and upstream of the resistivity transects did exhibit early-spring to mid-summer fluctuations up to 30 %.
Deleted: Figure 10
Deleted: Although the resistivity distribution across the pool remained systematically higher than the riffle throughout the entire monitoring period, both locations exhibited a dynamic response over the annual cycle. A greater
Deleted: number of measurements
Deleted: had to be
Deleted: of frozen-period data sets
Deleted: ,

846 ~~accompanied by higher model RMS errors.~~ A subset of the inverted resistivity models over the annual cycle (i.e.,
847 samples a–h identified in Fig. 9) are shown in Fig. 10. These snapshots capture the spatiotemporal evolution of
848 predominant geoelectrical conditions beneath the riverbed.

849 Spatial electrical resistivity data were highly variable across the pool (Fig. 10a–h). The highest resistivities were
850 observed along the south shoreline, which coincided with the presence of competent bedrock (Fig. 3b, i) ~~with~~
851 ~~bedding plane fractured and vertical joint sets.~~ Similarly resistive conditions extended southward onto the
852 floodplain. Subsurface conditions became less resistive toward the north shoreline, which coincided with the
853 presence of increased ~~vertical fracturing~~ and dissolution-~~enhanced~~ features, mechanically broken or weathered
854 bedrock, and a thin layer of organic rich sediment alongside the north shoreline and floodplain. Initial surveys
855 conducted across the pool on 25-Jul-2014 identified a relatively low resistivity zone (<1000 Ω m) extending 2 m
856 beneath the riverbed that spanned the full width of the river. Measurements on 26-Sep-2014 through 24-Dec-2014
857 captured the retraction of this zone toward the north shore. During this period the resistivity across the full transect
858 increased only slightly. The onset of frozen ground and river conditions on 29-Jan-2014 resulted in an abrupt shift
859 in the resistivity distribution. A high resistivity zone formed above the water table across the southern floodplain
860 and was accompanied by an increase in resistivity across the full river profile. It is important to note that these
861 frozen periods were accompanied by higher model RMS errors, and thus, our interpretation of these data focus on
862 long-period trends. The formation of river ice (~~visually observed~~ basal and surface ice) may have altered the true
863 geometry of the surface water body represented in the model, potentially contributing to the higher RMS errors
864 ~~along with the overall noisier measurements during this time (Fig. 9).~~ The arrival of seasonal thaw conditions on
865 27-Mar-2015 was accompanied by reduced resistivities across the river as rock and river ice progressively thawed
866 and was mobilized by spring freshet. Further seasonal warming on 6-May-2015 and 3-July-2015 resulted in a
867 systematic decrease in riverbed resistivity from the north to south shoreline.

Deleted: which may have contributed

Deleted: to the

Deleted: encountered during the winter period

Deleted: Fig. 10

Deleted: Fig. 11

Deleted: Fig. 11

Deleted: , with limited vertical and horizontal fractures

Deleted: fractures

868 Riverbed resistivity across the riffle portion of the river (Fig. 10a–h) was markedly different with respect to the
869 distribution and magnitude of resistivity fluctuations. The riffle exhibited a zone of comparatively low resistivity
870 (<100 Ω m) that extended slightly deeper than that at the pool, to a depth of 3 m. The initial survey on 26-Jul-2014
871 identified a zone of very low resistivity that progressively became more resistive over time (26-Sep-2014 through
872 24-Dec-2014). Much like the pool, however, this low resistivity zone reverted back toward the north shoreline. The
873 onset of seasonally frozen river conditions was accompanied by an increase in resistivity across a significant portion
874 of the riverbed. Inverse models during frozen water conditions were again accompanied by higher RMS errors,
875 which we attribute to the formation of river ice. ~~Unlike the pool, which experienced the formation of a substantial~~
876 zone of ground frost along the south shore, less ground frost was observed at depth along the riverbanks bounding
877 the riffle. Spring thaw brought reduced resistivities across the riverbed with subtle lateral variations, followed by
878 the beginnings of a less-resistive riverbed zone emanating southward from the north shoreline. The bedrock
879 resistivity below 3 m depth remained relatively constant through the monitoring period.

Deleted: Fig. 11

Deleted: which could not be accounted for in the model

880 4.3.2 Spatiotemporal Resistivity Trends

894 A resistivity index (RI) was calculated using Eq. (3) to compare spatiotemporal variations in electrical resistivity
895 within predefined zones of the bedrock beneath the river (Fig. 11); zones A and D represent conditions along the
896 south and north riverbank, while zones B and C represent conditions within the southern and northern portions the
897 river. These zones were defined based on their representative areas and the magnitude of the temporal fluctuations
898 observed over the full monitoring period (Fig. 10). A RI of zero indicates a mean zone resistivity (MZR) that is
899 equal to the mean annual resistivity (MAR) of the whole profile. An index of +1 indicates a resistivity that is twice
900 the annual mean, while an index of -0.5 indicates a resistivity that is half the annual mean.

Deleted: assess

Deleted: (Fig. 5)

Deleted: Fig. 12

Deleted: Fig. 11

901 The RI time-series for the pool (Fig. 11a) and riffle (Fig. 11b) capture the magnitude and frequency of the temporal
902 variability observed within these four zones. Relative to the MAR, the pool exhibited larger and more frequent
903 fluctuations in resistivity compared to the riffle. The south shoreline (zone A) at the pool was more dynamic than
904 the corresponding zone at the riffle; zone A at the pool encompasses a larger unsaturated zone, which is more likely
905 impacted by changes in temperature and saturation, especially during the freezing and thawing period. The north
906 shoreline (zone D) at the pool and riffle exhibited lower than average resistivities with relatively minimal transience
907 over the study period, with the exception of the mid-to-late-winter freeze-up. Here, a variable layer of sediment and
908 organic matter with higher water content likely moderated freeze-thaw fluctuations relative to sections of exposed
909 rock. Conditions below the riverbed (zones B and C) exhibited both longer-period (seasonal) and shorter-period
910 (intra-seasonal) fluctuations. While the relative changes observed at the pool were larger than the riffle, similar
911 seasonal trends were observed at each location. Zones B and C at the pool were mutually consistent, while those at
912 the riffle were less consistent.

Deleted: Fig. 12

Deleted: Fig. 12

Deleted: representative

Deleted: somewhat

913 Although perturbations were observed in the resistivity beneath the riverbed before and after winter freeze-up (e.g.,
914 zones B and C), the responses were dampened relative to the winter period. Events 13, 26 and 31 (Fig. 6), which
915 correspond to periods of increase precipitation, may coincide with observed perturbations in the RI; however, based
916 on these data it is not clear whether the riverbed resistivity and surface water responses are mutually consistent.
917 Here, a limited relationship may suggest that groundwater-surface water interaction does not occur in this section of
918 the river or that groundwater discharge is strong enough to limit potential groundwater-surface water mixing at this
919 particular location. Therefore, these observed geophysical dynamics within the riverbed may be more associated
920 with seasonal temperature transience with secondary influence due to solute-based fluctuations.

Deleted: significantly

Deleted: 4 and 7

Deleted: ;

Deleted: this

Deleted: correlation

Deleted: may

Deleted: discharge

Deleted: , and thus,

Deleted: ing

Deleted: , at least at the spatial scales considered in this study

Deleted: effects due to

Deleted: and

Deleted: low

Deleted: conditions

Deleted: , which varied with

921 5.0 Discussion

922 5.1 Influence of Water Properties on Formation Resistivity

923 Riverbed electrical resistivity mapping during low and high stage periods identified a spatiotemporal response
924 within the upper 6 m of rock with the southern cut bank exhibiting a reduction in resistivity while the remaining
925 portions of the river increased in resistivity. This spatiotemporal response, together with observed bedrock surface
926 conditions, indicates that riverbed morphology strongly impacts groundwater dynamics below the riverbed.

927 Long-term resistivity monitoring along the fixed profiles over the pool and riffle portions of the river revealed a
928 transient zone within the upper 2 m and 3 m of bedrock, respectively. In particular, the formation of a low

953 resistivity zone (high electrical conductivity) was observed during the warmer summer period that diminished as the
 954 environment cooled. While pore water conductivity depends on electrolytic concentration and temperature, their
 955 ~~independent variability could not~~ be decoupled across the entire study area given ~~in-situ sensor deployment~~
 956 limitations in a bedrock environment. Although this ~~uncertainty~~ in the driving mechanism of observed electrical
 957 changes below the riverbed hindered our ability to definitively define the vertical extent of a potential groundwater-
 958 surface water mixing zone, our geophysical data set does suggest that a groundwater-surface water mixing in a
 959 bedrock environment may be more limited, ~~due to the lower effective porosity of rock and heterogeneous and~~
 960 ~~anisotropic fracture distributions~~.

961 Aqueous temperature and specific conductance measurements collected in the river stage gauge (RSG1) and shallow
 962 bedrock well (SCV6) provided end-member conditions (Fig. 6). These data were used to assess the influence of
 963 aqueous conditions on bulk formation resistivity (Fig. 7). While some degree of overlap was observed between
 964 groundwater and surface water properties, they were generally differentiable across the study area. That being said,
 965 aqueous temperature fluctuations dominated the bulk electrical response over the full annual cycle. Given the
 966 impact of temperature on the bulk formation resistivity, observed bedrock resistivity dynamics are attributed to
 967 changes in water/rock temperature with secondary effects caused by changes in electrolytic concentration. These
 968 findings are consistent with Musgrave and Binley (2011), who concluded that temperature fluctuations over an
 969 annual cycle within a temperate wetland environment with groundwater electrical conductivities ranging from 400
 970 $\mu\text{S cm}^{-1}$ to 850 $\mu\text{S cm}^{-1}$ dominated formation resistivity transience. Of course, our annual temperature range was
 971 more extreme than that of Musgrave and Binley, we examined electrical dynamics within a ~~less-porous, more~~
 972 ~~heterogeneous and anisotropic~~ medium, and captured a broader range of seasonal conditions including ground frost
 973 and riverbed ice formation.

974 Measurements collected with a shorter time-step (diurnal) and shorter electrode spacing may have captured more
 975 transient rainfall or snowpack melt episodes focused along discrete fracture pathways, possibly leading to the
 976 identification of electrolytic-induced transients beneath the riverbed more indicative of a groundwater-surface water
 977 mixing zone. Based on the short-period of intraseasonal fluctuations observed in Fig. 11, and the timing and
 978 duration of major precipitation or thawing events (5 to 7 day cycles) (Fig.4), it is reasonable to assume that our
 979 geophysical time step (days to weeks) was accompanied by some degree of aliasing. Finally, it is possible that
 980 shallower sections of rock within the river exposed to direct sunlight during the day, which can vary depending on
 981 cloud cover (daily) and the sun's position in the sky (seasonally), may have exhibited a wider range, or more
 982 transient temperature fluctuations, than those areas beneath or adjacent to a canopy. A closer inspection of the
 983 unfrozen temporal response in zone B reveals a wider range in resistivity relative to the more northern zone C. At
 984 this latitude in the northern hemisphere the south shore will receive more direct sunlight; therefore, it is possible that
 985 the shallow rock on this side of the river experienced greater fluctuations in temperature (both seasonally and
 986 diurnally), thereby contributing to the observed geoelectrical dynamics. ~~Although diurnal fluctuations in surface~~
 987 ~~water temperature can be significant (>10°C) (e.g., Constantz et al. 1994; Constantz 1998), the relative effects of~~

- Deleted: individual contribution
- Deleted: to the bulk formation response cannot
- Deleted: inherent/practical
- Formatted: Font: Italic
- Deleted: in the number of direct measurement points
- Deleted: ambiguity
- Deleted: s
- Deleted: ,
- Deleted: in part by strong upward hydraulic gradients and groundwater discharge at this site.
- Deleted: Fig. 7
- Deleted: Fig. 8
- Deleted: likely

- Deleted: very different
- Deleted: (rock verses organic rich sediment),
- Deleted: ultimately
- Deleted: that
- Deleted: ed

- Deleted:
- Deleted: Fig. 12

1011 such transient temperature fluctuations on our geophysical measurements cannot be assessed given our more
1012 seasonally-scaled measurement sampling interval.

1013 5.2 Formation of Ground Frost and Anchor Ice

1014 A dramatic increase in bedrock resistivity was observed with the onset of freezing ground conditions; this can
1015 impact a wide range of infrastructure (e.g., dams, hydropower generation), ecologic (e.g., alteration of fish and
1016 benthic habitats) and hydraulic functions (e.g., river storage, baseflow) (Beltaos and Burrell 2015). The formation of
1017 a highly resistivity zone consistent with a seasonal frost front within the unsaturated portion of the riverbank (Fig.
1018 10e; zone A in Fig. 11a), and the accumulation of river ice resulted in marked changes in resistivity. These winter
1019 season effects are readily evident in Fig. 11 at the pool and riffle. Here, the magnitude of the resistivity increase
1020 may reflect a potential reduction in the hydraulic connectivity between surface water and groundwater during the
1021 winter months.

1022 Ground frost primarily formed along the riverbank over the southern floodplain at the pool. This topographically
1023 higher area was relatively devoid of large shrubs and trees (Fig. 2), and thus, likely experienced more severe weather
1024 conditions (e.g., higher winds resulted in less snow pack to insulate the ground). These conditions would promote,
1025 the formation of a thicker frost zone which propagated to the water table (pool in Fig. 10e). The adjacent northern
1026 riverbank and those up-gradient at the riffle were topographically lower (i.e., thinner unsaturated zone) and were
1027 sheltered by large trees. The formation of a seasonal frost zone along the riverbank may have implications to
1028 baseflow dynamics during the winter months and early-thaw period.

1029 A simple sensitivity analysis of the inversion process using different constraints on surface water geometry and
1030 aqueous electrical resistivity indicated that model convergence was highly sensitive to surface water geometry and
1031 aqueous resistivity. For instance, setting an aqueous resistivity of one-half the true value led to poor model
1032 convergence and unrealistic resistivity values for bedrock. The riffle was relatively less sensitive to surface water
1033 properties likely because of its overall lower river stage compared to the pool, and hence, relatively lower impact of
1034 the surface water body on the apparent resistivity measurement. This sensitivity to surface water properties is a
1035 consequence of the high electrical conductivity of the surface water relative to high resistivity bedrock.

1036 Anchor ice reduced the electrical connectivity across the riverbed, while the ice crust along the surface of the water
1037 altered the effective geometry of the water body, further influencing the inverse solution. While the formation of
1038 river ice was accompanied by higher RMS errors at the pool (>6 %) and riffle (>4 %) (Fig. 9), direct measurements
1039 of river ice thickness and spatial extent could not be collected, and thus explicitly incorporated into the surface water
1040 layer geometry during the winter months.

1041 5.3 Implications to the Conceptualization of Groundwater-Surface Water Exchange in Bedrock Rivers

1042 The fractured dolostone in this study consists of a visible orthogonal joint network approximately orientated at 10°
1043 to 20° NNE and 280° to 290° SNW, consistent with the regional joint orientations, with frequencies ranging from
1044 centimeter to sub-meter scale where exposed at surface. Streambed resistivity measurements indicate a seasonally

Deleted: Fig. 11

Deleted: Fig. 12

Deleted: Fig. 12

Deleted: T

Deleted: observed at the pool and riffle

Deleted: suggest

Deleted: vegetation

Deleted: likely

Deleted: enhanced

Deleted: Fig. 11

Moved down [2]: The presence of river ice did have a noticeable impact on the inverse model results as reflected in the higher RMS errors at the pool (>6 %) and riffle (>4 %) during the winter period (Fig. 10). This was particularly evident at the pool, which exhibited a more uniform high resistivity zone beneath the riverbed (Fig. 11e).

Deleted: suggests

Deleted: dependent

Deleted: on

Deleted: its actual

Deleted: applying

Deleted: very

Deleted: substantial overestimates

Deleted: of river resistivity

Deleted: contrast between the conductive surface water and resistive bedrock

Deleted: further

Deleted: thereby

Deleted: impacting

Moved (insertion) [2]

Deleted: T

Deleted: presence

Deleted: did have a noticeable impact on the inverse model results as reflected in the

Deleted: during the winter period

Deleted: Fig. 10

Deleted: .

Deleted: This was particularly evident at the pool, which exhibited a more uniform high resistivity zone beneath the riverbed (Fig. 11e). Unfortunately,

Deleted: were

Deleted: thus could not be

Deleted: conceptualization

Deleted: Nevertheless, the effect of ...

1096 dynamic groundwater zone within the upper 2 m to 3 m of riverbed. A less-resistive zone (<1000 Ω m) was
1097 observed beneath the pool emanating from the north shoreline during warmer low-flow periods (July and August
1098 2014). This zone retracted in late-summer but showed signs of reappearance in early July 2015. A similarly
1099 evolving low-resistivity zone (<100 Ω m) was observed across the riffle, but was more variable across the river
1100 transect. Although dynamic fluctuations in temperature and aqueous conductivity support the potential existence of
1101 a groundwater-surface water mixing zone, it is not yet clear how these geoelectrical dynamics were influenced or
1102 enhanced by fluid flow in the discrete fractures, exchange between the mobile and immobile pore-phase, and
1103 seasonal thermal gradients across the riverbed.

Deleted:

Deleted: While

Deleted: definitive

Deleted: or

1104 Discrete fracture networks and dissolution-enhanced features will result in a more heterogeneous and anisotropic
1105 groundwater-surface water mixing zones compared to porous unconsolidated sediment. Swanson and Cardenas
1106 (2010) examined the utility of using heat as a tracer of groundwater-surface water exchange across a pool-riffle-pool
1107 sequence. Observed thermal patterns and zones of influence (i.e., effective mixing zones) in their study were
1108 consistent with conceptual models depicting a pool-riffle-pool sequence. While similar temperature dynamics may
1109 be expected across the pool-riffle-pool sequence in a bedrock environment, our coarser temporal sampling interval
1110 (days to weeks) combined with our smoothed resistivity models limited our ability to capture subtle diel temperature
1111 transience across discrete fractures or flow features. Although the electrical resistivity method was not able to
1112 definitively differentiate between groundwater and surface water, our geophysical measurements do provide insight
1113 into the magnitude, lateral extent and spatiotemporal scale of geoelectrical transience, which are largely driven by
1114 temperature fluctuations within the upper few meters of rock.

Deleted: While groundwater-surface water exchange within a fractured bedrock river are expected,

Deleted: d

Deleted: will

Deleted: support

Deleted: more

Deleted: resolve a groundwater-surface water mixing zone

Deleted: these

Deleted: data

1115 6.0 Conclusions

1116 Induced resistivity measurements collected across a 200 m reach of the Eramosa River during low and high-stage
1117 periods showed that spatiotemporal variations in resistivity will be dependent upon riverbed morphology, i.e., the
1118 exposure of bedding plane and vertical fractures, and competency of the rock surface. Complementary fracture and
1119 temperature profiling within the open and lined borehole revealed abundant active groundwater flow zones spanning
1120 the upper 8-10 m of bedrock, with strong intra-seasonal and seasonal temperature variations along horizontal
1121 fracture sets. While surface resistivity profiles captured geoelectrical dynamics within the upper few meters of rock,
1122 these data represent indirect evidence of riverbed transience resulting from changes in groundwater temperature and
1123 specific conductance. Geoelectrical transience was primarily governed by seasonal temperature trends with
1124 secondary effects arising from porewater conductance; however, spatiotemporal variations in temperature and
1125 specific conductance could not be decoupled beyond the fixed monitoring points.

Deleted: Electrical resistivity methods were used to investigate the temporal geoelectrical response beneath a bedrock river within the upper 6 meters of rock over a full annual cycle.

Deleted: the

Deleted: r

Deleted: and low flow

Deleted: conditions

Deleted: were

1126 Time-lapse electrical resistivity imaging of the pool and riffle portion of the river, sampled on a semi-daily to semi-
1127 weekly interval, showed consistently higher resistivity at the pool with more elevated resistivities along the south
1128 shoreline. Seasonal cooling was accompanied by the formation of a higher-resistivity zone emanating from the
1129 south shore to north shore in both the pool and riffle. This resistivity trend reversed during the seasonal warming
1130 cycle, becoming less-resistive toward the south shoreline as seasonal temperatures increased and river stage
1131 decreased. The formation of ground frost and basal ice along the riverbed had a strong impact on the seasonal

Deleted:

1158 resistivity profiles during the winter months. Intraseasonal geoelectrical transience associated with major
 1159 precipitation events, which were accompanied by short-period perturbations in surface water temperature and
 1160 specific conductance had a relatively small impact on sub-riverbed resistivity. This could be explained by a
 1161 seasonally-sustained groundwater discharge zone across this reach of the river, which would have limited or
 1162 moderated electrical resistivity changes associated with surface water mixing with groundwater. The formation of a
 1163 transient 2 m thick low-resistivity zone within the pool in mid-summer appears to be associated with an increase in
 1164 surface water/bedrock formation temperatures during low river stage. During this time, the riffle was characterized
 1165 by a 3 m thick low-resistivity zone spanning the entire width of the river, underlain by more resistive material.
 1166 These lower resistivities at the riffle suggest the presence of more porous bedrock consistent with dissolution-
 1167 enhanced rock and/or a layer of weathered bedrock zone overlying more competent bedrock.

1168 Spatiotemporal resistivity dynamics were governed by riverbed morphology together with seasonal changes in water
 1169 temperature and electrolytic concentration. During the winter, ground frost and basal ice along the riverbed
 1170 strongly influenced the electrical resistivity across the riverbed. Observed intraseasonal (i.e., spring, summer, fall)
 1171 geoelectrical changes beneath the riverbed were strongly dependent upon seasonal temperature trends, with the pool
 1172 and riffle exhibiting variable horizontal and vertical zones of influence. While the riverbed resistivity was highly
 1173 susceptible to seasonal atmospheric temperature trends, such transience could have implications to biogeochemical
 1174 processes, benthic activity, and macro-scale hyporheic zone processes.

1175 This study demonstrates that surface electrical resistivity has the capacity to detect and resolve changes in electrical
 1176 resistivity due to transience in temperature and specific conductance within a shallow bedrock river over a complete
 1177 annual cycle. Imaging the magnitude and scale of transience within the riverbed will be critical to the advancement
 1178 of our understanding of mechanisms controlling groundwater-surface water exchange within fractured bedrock
 1179 rivers. Given the challenges and costs associated with installing sensors within rock and effectively sampling a
 1180 heterogeneous flow system, minimally invasive surface and borehole geophysical methods offer an ideal alternative,
 1181 and possibly more effective approach for long-term groundwater-surface water monitoring of bedrock environments
 1182 by reducing instrumentation costs and impacts to ecosensitive environments.

Deleted: seasonally

Deleted: flux

Deleted: Conversely

Deleted: a

Deleted: material

Deleted: enhanced-

Deleted: of

Deleted: ¶
 Although seasonal geoelectrical dynamics were observed at both the pool and riffle, the pool was more transient and exhibited a broader range, yet spatially more uniform distribution in resistivity. Conversely, the riffle exhibited more lateral variability in resistivity along across the riverbed. Seasonal cooling was accompanied by a higher-resistivity zone emanating from the south shore to north shore in both the pool and riffle. This resistivity trend reversed during the seasonal warming cycle, becoming less-resistive toward the south shoreline as seasonal temperatures increased and river flow decreased. The formation of ground frost and basal ice along the riverbed had a strong and sometimes negative impact on the seasonal resistivity profiles during the winter months. Intraseasonal geoelectrical transience associated with major precipitation events, which were accompanied by short-period perturbations in surface water temperature and specific conductance had a relatively small impact on riverbed resistivity. This may be explained by the presence of a strong groundwater discharge zone across this reach of the river, which may have limited or moderated the electrical resistivity changes within the suspected groundwater-surface water mixing zone.¶

Deleted: Time-lapse temperature profiling within the angled borehole underlying the river revealed active groundwater flow zones. While our resistivity measurements captured geoelectrical dynamics within the upper few meters of riverbed, these data are indirect evidence of a groundwater surface water mixing zone; whether the observed geoelectrical transience are primarily a function of seasonal temperature fluctuations or transience in ionic ...

Deleted: our

Deleted: within a bedrock riverbed

Deleted: .

Deleted: Given the complex fracture distribution, geometry and dissolution features inherent to sedimentary rock, surface resistivity methods may be mos ...

Formatted: Font: Not Bold, Not All caps

1264 **DATA AVAILABILITY**

1265 The data used in this study are presented in the figures. Complete monitoring data sets (Figures 9 and 10) and can be
1266 made available upon request from the corresponding author.

1267

1268 **TEAM LIST**

1269 **Steelman, Kennedy, Capes, Parker**

1270

1271 **AUTHOR CONTRIBUTION**

1272 **Steelman** designed the experiment, conducted the surveys, and analysed the geophysical data; **Kennedy** designed
1273 the borehole network, logged the core, instrumented the hydrological monitoring network; **Capes** designed and
1274 collected the temperature profiles, logged the core and supported hydrological data collection and interpretation;
1275 **Parker** contributed to the design of the hydrological geophysical monitoring network, and supported conceptual
1276 understanding of groundwater flow through fractured rock.

1277

1278 **COMPETING INTERESTS**

1279 The authors declare that they have no conflict of interest.

1280

1281 **ACKNOWLEDGEMENTS**

1282 This research was made possible through funding by the Natural Sciences and Engineering Research Council of
1283 Canada in the form of a Banting Fellowship to Dr. Steelman, and an Industrial Research Chair (Grant #
1284 IRCPJ363783-06) to Dr. Parker. The authors are very appreciative of the field contributions of staff and students at
1285 the University of Guelph and University of Waterloo, particularly field-technicians Dan Elliot and Bob Ingleton.
1286 This work would not have been possible without land-access agreements with Scouts Canada, Ontario Ministry of
1287 Natural Resources, and river-flow data provided by the Grand River Conservation Authority.

1288

1289 **REFERENCES**

- 1290 Alexander, M. D. and Caissie, D.: Variability and comparison of hyporheic water temperatures and seepage fluxes
1291 in a small Atlantic Salmon stream, *Groundwater*, 41, 72-82, 2003.
- 1292 Anderson, M. P.: Heat as a ground water tracer, *Ground Water*, 43, 951-968, 2005.
- 1293 Archie, G. E.: The electrical resistivity log as an aid in determining some reservoir characteristics, *T. Am. Inst.*
1294 *Mineral. Metall. Petrol. Eng.*, 146, 54-62, 1942.
- 1295 Arps, J. J.: The effect of temperature on the density and electrical resistivity of sodium chloride solutions, *Trans.*
1296 *A.I.M.E.*, 164, 54-62, 1953.
- 1297 Beltaos, S. and Burrell, B. C.: Hydrotechnical advances in Canadian river ice science and engineering during the
1298 past 35 years, *Can. J. Civ. Eng.*, 42, 583-591, dx.doi.org/10.1139/cjce-2014-0540, 2015.
- 1299 Bianchin, M. S., Smith, L., and Beckie, R. D.: Defining the hyporheic zone in a large tidally influenced river, *J.*
1300 *Hydrol.*, 406, 16-29, doi:10.1016/j.jhydrol.2011.05.056, 2011.
- 1301 Binley, A., Ullah, S. Heathwaite, A. L., Heppell, C., Byrne, P., Lansdown, K., Trimmer, M., and Zhang, H.:
1302 Revealing the spatial variability of water fluxes at the groundwater-surface water interface, *Water Resour. Res.*, 49,
1303 3978-3992, doi:10.1002/wrcr.20214, 2013.
- 1304 Boano, F., Revelli, R., and Ridolfi L.: Reduction of the hyporheic zone volume due to the stream-aquifer interaction,
1305 *Geophys. Res. Lett.*, 35, L09401, doi:10.1029/2008GL033554, 2008.
- 1306 Brassington, R.: *Field Hydrogeology*, John Wiley & Sons, Inc, 1998.
- 1307 Briggs, M. A., Lautz, L. K., McKenzie, J. M., Gordon, R. P., and Hare, D. K.: Using high-resolution distributed
1308 temperature sensing to quantify spatial and temporal variability in vertical hyporheic flux, *Water Resour. Res.*, 48,
1309 W02527, doi:10.1029/2011WR011227, 2012.
- 1310 Brunton, F. R.: Update of revisions to the Early Silurian stratigraphy of the Niagara Escarpment: integration of
1311 sequence stratigraphy, sedimentology and hydrogeology to delineate hydrogeologic units, In *Summary of Field*
1312 *Work and Other Activities 2009*, Ontario Geologic Survey, Open File Report 6240, pp. 25-1 to 25-20, 2009.
- 1313 Campbell, R. B., Bower, C. A., and Richards, L. A.: Change of electrical conductivity with temperature and the
1314 relation of osmotic pressure to electrical conductivity and ion concentration for soil extracts, *Soil Sci. Soc. Am.*
1315 *Proc.*, 12, 66-69, 1948.
- 1316 Cardenas, M. B. and Markowski, M. S.: Geoelectrical imaging of hyporheic exchange and mixing of river water and
1317 groundwater in a large regulated river, *Environ. Sci. Technol.*, 45, 1407-1411, dx.doi.org/10.1021/es103438a, 2011.
- 1318 Cole, J., Coniglio, M., and Gautrey, S.: The role of buried bedrock valleys on the development of karstic aquifers in
1319 flat-lying carbonate bedrock: insights from Guelph, Ontario, Canada, *Hydrogeol. J.*, 17, 1411-1425,
1320 doi:10.1007/s10040-009-0441-3, 2009.

1321 | [Constantz, J.: Interaction between stream temperature, streamflow, and groundwater exchanges in alpine streams,](#)
1322 | [Water Resour. Res., 34, 1609-1615, 1998.](#)

1323 | Conant Jr., B.: Delineating and quantifying ground water discharge zones using streambed temperature,
1324 | Groundwater, 42, 243-257, 2004.

1325 | [Constantz, J., Thomas, C.L., and Zellweger, G.: Influence of diurnal variations in stream temperature on streamflow](#)
1326 | [lows and groundwater recharge, Water Resour. Res., 30, 3253-3264, 1994](#)

1327 | Constantz, J.: Heat as a tracer to determine streambed water exchanges, Water Resour. Res., 44, W00D10, doi:
1328 | 10.1029/2008WR006996, 2008.

1329 | Coscia, I., Greenhalgh, S. A., Linde, N., Doetsch, J., Marescot, L., Günther, T., Vogt, T., and Green, A. G.: 3D
1330 | crosshole ERT for aquifer characterization and monitoring of infiltrating river water, Geophysics, 76, G49-G59, doi:
1331 | 10.1190/1.3553003, 2011.

1332 | Coscia, I., Linde, N., Greenhalgh, S., Vogt, T., and Green, A.: Estimating traveltimes and groundwater flow pattern
1333 | using 3D time-lapse crosshole ERT imaging of electrical resistivity fluctuations induced by infiltrating river water,
1334 | Geophysics, 77(4), E239-E250, doi: 10.1190/GEO2011-0328.1, 2012.

1335 | Crook, N., Binley, A., Knight, R., Robinson, D. A., Zarnetske J., and Haggerty, R.: Electrical resistivity imaging of
1336 | the architecture of substream sediments, Water Resour. Res., 44, W00D13, doi:10.1029/2008WR006968, 2008.

1337 | Crosbie, R. S., Taylor, A. R., Davis, A. C., Lamontagne, S., and Munday, T.: Evaluation of infiltration from losing-
1338 | disconnected rivers using a geophysical characterisation of the riverbed and a simplified infiltration model, J.
1339 | Hydrol., 508, 102-113, <http://dx.doi.org/10.1016/j.jhydrol.2013.07.045>, 2014.

1340 | Dimova, T. N., Swarzenski, P.W., Dulaiova, H., and Glenn, C. R.: Utilizing multichannel electrical resistivity
1341 | methods to examine the dynamics of the fresh water-seawater interface in two Hawaiian groundwater systems, J.
1342 | Geophys. Res., 117, C02012, doi: 10.1029/2011JC007509, 2012.

1343 | Doetsch, J., Linde, N., Vogt, T., Binley, A., and Green, A. G.: Imaging and quantifying salt-tracer transport in a
1344 | riparian groundwater system by means of 3D ERT monitoring, Geophysics, 77, B207-B218, doi:10.1190/GEO2012-
1345 | 0046.1, 2012.

1346 | Doro, K. O., Leven, C., and Cirpka, O. A.: Delineating subsurface heterogeneity at a loop of River Steinlach using
1347 | geophysical and hydrogeological methods, Environ. Earth Sci., 69, 335-348, doi:10.1007/s12665-013-2316-0, 2013.

1348 | Ellis, D.V.: Well logging for earth scientists, Elsevier Science Publishing Company, Inc, 1987.

1349 | Evans, E. C., Greenwood, M. T., and Petts, G. E.: Thermal profiles within river beds, Hydrol. Process., 9, 19-25,
1350 | 1995.

1351 Fan, Y., Toran, L., and Schlische, R. W.: Groundwater flow and groundwater-stream interaction in fractured and
1352 dipping sedimentary rocks: insights from numerical models, *Water Resour. Res.*, 43, W01409,
1353 doi:10.1029/2006WR004864, 2007.

1354 Froese, D. G., Smith, D. G., and Clement, D. T.: Characterizing large river history with shallow geophysics: middle
1355 Yukon River, Yukon Territory and Alaska, *Geomorphology*, 67, 391-406, doi:10.1016/j.geomorph.2004.11.011,
1356 2005.

1357 Glover, P. W. J.: A generalized Archie's law for n phases, *Geophysics*, 75, E247-E265, doi: 10.1190/1.3509781,
1358 2010.

1359 Gourry, J-C., Vermeersch, F., Garcin, M., and Giot, D.: Contribution of geophysics to the study of alluvial deposits:
1360 a case study in the Val d'Avaray area of the River Loire, France, *J. Appl. Geophys.*, 54, 35-49, doi:
1361 10.1016/j.jappgeo.2003.07.002, 2003.

1362 Harrington, G. A., Gardner, W. P., and Munday, T. J.: Tracking groundwater discharge to a large river using tracers
1363 and geophysics, *Groundwater*, 52, 837-852, doi:10.1111/gwat.12124, 2014.

1364 Hatch, C. E., Fisher, A. T., Revenaugh, J. S., Constantz, J., and Ruehl, C.: Quantifying surface water-groundwater
1365 interactions using time series analysis of streambed thermal records: Method development, *Water Resour. Res.*, 42,
1366 W10410, doi:10.1029/2005WR004787, 2016.

1367 Irvine, D. J., Briggs, M. A., Lautz, L. K., Gordon, R. P., McKenzie, J. M., and Cartwright, I.: Using diurnal
1368 temperature signals to infer vertical groundwater-surface water exchange, *Groundwater*, version of record online 3-
1369 Oct-2016, doi: 10.1111/gwat.12459, 2016.

1370 Johnson, T. C., Slater, L. D., Ntarlagiannis, D., Day-Lewis, F. D., and Elwaseif, M.: Monitoring groundwater-
1371 surface water interaction using time-series and time-frequency analysis of transient three-dimensional electrical
1372 resistivity changes, *Water Resour. Res.*, 48, W07506, doi:10.1029/2012WR011893, 2012.

1373 Käser, D. H., Binley, A., and Heathwaite, A. L.: On the importance of considering channel microforms in
1374 groundwater models of hyporheic exchange, *River Res. Applic.*, 29, 528-535, doi:10.1002/rra.1618, 2013.

1375 Keery, J., Binley, A., Crook, N., and Smith, J. W. N.: Temporal and spatial variability of groundwater-surface water
1376 fluxes: Development and application of an analytical method using temperature time series, *J. Hydrol.*, 336, 1-16,
1377 doi:10.1016/j.jhydrol.2006.12.003, 2007.

1378 Keller, G. V.: Section V: Electrical properties, In Carmichael, R.S., ed., *CRC Practical handbook of physical
1379 properties of rock and minerals*, CRC Press, 361-427, 1989.

1380 Keller, C., Cherry, J. A., and Parker, B. L.: New method for continuous transmissivity profiling in fractured rock,
1381 *Groundwater*, 52, 352-367, doi:10.1111/gwat.12064, 2014.

1382 Knight, R. J. and Endres, A. L.: Chapter 3: An Introduction to Rock Physics Principles for Near-Surface
1383 Geophysics, In Butler, D.K., ed., Near-Surface Geophysics, Society of Exploration Geophysics, Tulsa, Oklahoma,
1384 31-70, 2005.

1385 Kunert, M., Coniglio, M., and Jowett, E. C.: Controls and age of cavernous porosity in Middle Silurian dolomite,
1386 southern Ontario, Can. J. Earth Sci., 35, 1044-1053, 1998.

1387 Kunert, M. and Coniglio, M.: Origin of vertical shafts in bedrock along the Eramosa River valley near Guelph,
1388 southern Ontario, Can. J. Earth Sci., 39, 43-52, doi:10.1139/E01-053, 2002.

1389 Lemieux, J-M., Kirkwood, D., and Therrien, R.: Fracture network analysis of the St-Eustache quarry, Quebec,
1390 Canada, for groundwater resources management, Can. Geotech. J., 46, 828-841, 2009.

1391 [Loke M.H.: Tutorial: 2-D and 3-D electrical imaging surveys, Geotomo Software, Malaysia, 2002.](#)

1392 Loke, M. H. and Dahlin, T.: A comparison of the Gauss-Newton and quasi-Newton methods in resistivity imaging
1393 inversion, J. Appl. Geophys., 49, 149-162, 2002.

1394 Loke, M. H., Chambers, J. E., Rucker, D. F., Kuras, O., and Wilkinson, P. B.: Recent developments in the direct-
1395 current geoelectrical imaging method, J. Appl. Geophys., 95, 135-156,
1396 <http://dx.doi.org/10.1016/j.jappgeo.2013.02.017>, 2013.

1397 McLaren, R. G., Sudicky, E. A., Park, Y-J., and Illman, W. A.: Numerical simulation of DNAPL emissions and
1398 remediation in a fractured dolomitic aquifer, J. Contam. Hydrol., 136-137, 56-71,
1399 doi:10.1016/j.jconhyd.2012.05.002, 2012.

1400 McNeill, J. D.: Electromagnetic terrain conductivity measurement at low induction numbers, Geonics Ltd. Technical
1401 Note, TN-6, 1980.

1402 Meyer, J. R., Parker, B. L., and Cherry, J. A.: Detailed hydraulic head profiles as essential data for defining
1403 hydrogeologic units in layered fractured sedimentary rock, Environ. Geol., 56, 27-44, doi:10.1007/s00254-007-
1404 1137-4, 2008.

1405 Meyerhoff, S. B., Karaoulis, M., Fiebig, F., Maxwell, R. M., Revil, A., Martin, J. B., and Graham, W. D.:
1406 Visualization of conduit-matrix conductivity differences in a karst aquifer using time-lapse electrical resistivity,
1407 Geophys. Res. Lett., 39, L24401, doi:10.1029/2012GL053933, 2012.

1408 Meyerhoff, S. B., Maxwell, R. M., Revil, A., Martin, J. B., Karaoulis, M., and Graham, W. D.: Characterization of
1409 groundwater and surface water mixing in a semiconfined karst aquifer using time-lapse electrical resistivity
1410 tomography, Water Resour. Res., 50, doi:10.1002/2013WR013991, 2014.

1411 Miller, C. R., Routh, P. S., Brosten, T. R., and McNamara, J. P.: Application of time-lapse ERT imaging to
1412 watershed characterization, Geophysics, 73, G7-G17, doi: 10.1190/1.2907156, 2008.

- 1413 Musgrave, H. and Binley, A.: Revealing the temporal dynamics of subsurface temperature in a wetland using time-
1414 lapse geophysics, *J. Hydrol.*, 396, 258-266, doi: 10.1016/j.jhydrol.2010.11.008, 2011.
- 1415 Naegeli, M. W., Huggenberger, P., and Uehlinger, U.: Ground penetrating radar for assessing sediment structures in
1416 the hyporheic zone of a prealpine river, *J.N. Am. Benthol. Soc.*, 15, 353-366, 1996.
- 1417 Norman, F. A. and Cardenas, M. B.: Heat transport in hyporheic zones due to bedforms: An experimental study,
1418 *Water Resour. Res.*, 50, 3568-3582, doi:10.1002/2013WR014673, 2014.
- 1419 Novakowski, K. S. and Lapcevic, P. A.: Regional hydrogeology of the Silurian and Ordovician sedimentary rock
1420 underlying Niagara Falls, Ontario, Canada, *J. Hydrol.*, 104, 211-236, 1998.
- 1421 Nyquist, J., Freyer, P. A., and Toran, L.: Stream bottom resistivity tomography to map ground water discharge,
1422 *Ground Water*, 46, 561-569, doi:10.1111/j.1745-6584.2008.00432.x, 2008.
- 1423 Orlando, L.: Some consideration on electrical resistivity imaging for characterization of waterbed sediments, *J.*
1424 *Appl. Geophys.*, 95, 77-89, doi:10.1016/j.jappgeo.2013.05.005, 2013.
- 1425 Oxtobee, J. P. A. and Novakowski, K.: A field investigation of groundwater/surface water interaction in a fractured
1426 bedrock environment, *J. Hydrol.*, 269, 169-193, 2002.
- 1427 Oxtobee, J. P. A. and Novakowski, K. S.: Ground water/surface water interaction in a fractured rock aquifer,
1428 *Groundwater*, 41(5), 667-681, 2003.
- 1429 Pehme, P. E., Parker, B. L., Cherry, J. A., and Greenhouse, J. P.: Improved resolution of ambient flow through
1430 fractured rock with temperature logs, *Groundwater*, 48, 191-205, doi:10.1111/j.1745-6584.2009.00639.x, 2010.
- 1431 Pehme, P. E., Parker, B. L., Cherry, J. A., and Blohm, D.: Detailed measurement of the magnitude and orientation of
1432 thermal gradients in lined corehole/coreholes for characterizing groundwater flow in fractured rock, *J. Hydrol.*, 513,
1433 101-114, <http://dx.doi.org/10.1016/j.jhydrol.2014.03.015>, 2014.
- 1434 Perrin, J., Parker, B. L., and Cherry, J. A.: Assessing the flow regime in a contaminated fractured and karstic
1435 dolostone aquifer supplying municipal water, *J. Hydrol.*, 400, 396-410, doi:10.1016/j.jhydrol.2011.01.055, 2011.
- 1436 Reynolds, J.M.: *An Introduction to Applied and Environmental Geophysics* (2nd edition), John Wiley & Sons, 2011.
- 1437 Rhoades, J. D., Raats, P. A. C., and Prather, R. J.: Effect of liquid-phase electrical conductivity, water content, and
1438 surface conductivity on bulk soil electrical conductivity, *Soil Sci. Soci. Am. J.*, 40, 651-655, 1976.
- 1439 Rucker, D. F., Noonan, G. E., and Greenwood, W. J.: Electrical resistivity in support of geological mapping along
1440 the Panama Canal, *Eng. Geol.*, 117, 121-133, 2011.
- 1441 Sambuelli, L., Leggieri, S., Calzoni, C., and Porporato, C.: Study of riverine deposits using electromagnetic methods
1442 at a low induction number, *Geophysics*, 72(5), B113-B120, doi:10.1190/1.2754249, 2007.

1443 Schmidt, C., Conant Jr., B., Bayer-Raich, M., and Schirmer, M.: Evaluation and field-scale application of an
1444 analytical method to quantify groundwater discharge using mapped streambed temperatures, *J. Hydrol.*, 347, 292-
1445 307, doi:10.1016/j.jhydrol.2007.08.022, 2007.

1446 Silliman, S. E. and Booth, D. F.: Analysis of time-series measurements of sediment temperature for identification of
1447 gaining vs. losing portions of Juday Creek, Indiana, *J. Hydrol.*, 146, 131-148, 1993.

1448 Singha, K., Day-Lewis, F. D., Johnson, T., and Slater, L. D.: Advances in interpretation of subsurface processes
1449 with time-lapse electrical imaging, *Hydrol. Process.*, 29, 1549-1576, doi:10.1002/hyp.10280, 2015.

1450 Singha, K., Pidlisecky, A., Day-Lewis, F. D., and Gooseff, M. N. Electrical characterization of non-Fickian
1451 transport in groundwater and hyporheic systems, *Water Resour. Res.*, 44, W00D07, doi:10.1029/2008WR007048,
1452 2008.

1453 Sirieix, C., Riss, J., Rey, F., Prétou, F., and Lastennet, R.: Electrical resistivity tomography to characterize a karstic
1454 Vauclusian spring: Fontaine d'Orbe (Pyrénées, France), *Hydrogeol. J.*, 22, 911-924, doi:10.1007/s10040-013-1095-
1455 8, 2014.

1456 [Slater, L., Binley, A.M., Daily, W., and Johnson, R.: Cross-hole electrical imaging of a controlled saline tracer
1457 injection, *J. Appl. Geophys.*, 44, 85-102, 2000.](#)

1458 Slater, L. D., Ntarlagiannis D., Day-Lewis, F. D., Mwakanyamale, K., Versteeg, R. J., Ward, A., Strickland, C.,
1459 Johnson, C. D., and Lane Jr. J. W.: Use of electrical imaging and distributed temperature sensing method to
1460 characterize surface water-groundwater exchange regulating uranium transport at the Hanford 300 Area,
1461 Washington, *Water Resour. Res.*, 46, W10533, doi:10.1029/2010WR009110, 2010.

1462 Snieder, R. and Trampert, J.: Inverse problems in geophysics, In Wirgin A. (ed), *Wavefield Inversion*, Springer-
1463 Verlag, New York, pp 119-190, 1999.

1464 Stickler, M. and Alfredsen, K. T.: Anchor ice formation in streams: a field study, *Hydrol. Process.*, 23, 2307-2315,
1465 doi:10.1002/hyp.7349, 2009.

1466 Steelman, C. M., Kennedy, C. S., and Parker, B. L.: Geophysical conceptualization of a fractured sedimentary
1467 bedrock riverbed using ground-penetrating radar and induced electrical conductivity, *J. Hydrol.*, 521, 433-446,
1468 <http://dx.doi.org/10.1016/j.jhydrol.2014.12.001>, 2015a.

1469 Steelman, C. M., Parker, B. L., and Kennedy, C. S.: Evaluating local-scale anisotropy and heterogeneity along a
1470 fractured sedimentary bedrock river using EM azimuthal resistivity and ground-penetrating radar, *J. Appl. Geophys.*,
1471 116, 156-166, <http://dx.doi.org/10.1016/j.jappgeo.2015.03.003>, 2015b.

1472 Swanson, T. E. and Cardenas, M. B.: Diel heat transport within the hyporheic zone of a pool-riffle-pool sequence of
1473 a losing stream and evaluation of models for fluid flux estimation using heat, *Limnol. Oceanogr.*, 55, 1741-1754,
1474 doi: 10.4319/lo.2010.55.4.1741, 2010.

1475 Tinkler, K.J. and Wohl E.E.: Rivers over rock: fluvial processes in bedrock channels. Geophysical Monograph 17,
1476 American Geophysical Union, Washington, D.C, 1998.

1477 Toran, L., Nyquist J. E., Fang, A. C., Ryan, R. J., and Rosenberry, D. O.: Observing lingering hyporheic storage
1478 using electrical resistivity: variations around stream restoration structures, Crabby Creek, PA, Hydrol. Process. 27,
1479 1411-1425, doi: 10.1002/hyp.9269, 2013a.

1480 Toran, L., Hughes, B. Nyquist, J. and Ryan, R.: Freeze core sampling to validate time-lapse resistivity monitoring of
1481 the hyporheic zone, Groundwater, 51, 635-640, doi: 10.1111/j.1745-6584.2012.01002.x, 2013b.

1482 Wallin, E. L., Johnson, T. C., Greenwood, W. J., and Zachara, J. M.: Imaging high stage river-water intrusion into a
1483 contaminated aquifer along a major river corridor using 2-D time-lapse surface electrical resistivity tomography,
1484 Water Resour. Res., 49, 1693-1708, doi: 10.1002/wrcr.20119, 2013.

1485 Ward, A. S., Gooseff, M. N., and Singha, K.: Imaging hyporheic zone solute transport using electrical resistivity,
1486 Hydrol. Process., 24, 948-953, doi: 10.1002/hyp.7672, 2010a

1487 Ward, A. S., Gooseff, M. N., and Singha, K.: Characterizing hyporheic transport processes – interpretation of
1488 electrical geophysical data in coupled stream-hyporheic zone systems during solute tracer studies, Adv. Water.
1489 Resour., 33, 1320-1330, doi: 10.1016/j.advwatres.2010.05.008, 2010b.

1490 Ward, A. S., Fitzgerald, M., Gooseff, M. N., Voltz, T. J., Binley, A. M., and Singha, K.: Hydrologic and geomorphic
1491 controls on hyporheic exchange during base flow recession in a headwater mountain stream, Water Resour. Res., 48,
1492 W04513, doi: 10.1029/2011WR011461, 2012.

1493 Waxman, M. H. and Smits, L. J. M.: Electrical conductivities in oil-bearing shaly sands, Soc. Petrol. Eng. J., 8, 107-
1494 122, 1968.

1495 White, D. S., Elzinga, C. H., and Hendricks, S. P.: Temperature patterns within the hyporheic zone of a northern
1496 Michigan river, J. N. Am. Benthol. Soc., 6(2), 85-91, 1987.

1497 Woessner, W. W.: Stream and fluvial plain ground water interactions: rescaling hydrogeologic thought,
1498 Groundwater, 38(3), 423-429, 2000.

1499 Worthington, P. F.: The uses and abuses of the Archie equations, 1: The formation facture-porosity relationship, J.
1500 Appl. Geophys. 30, 215-228, 1993

1501 Zanini, L., Novakowski, K. S., Lapcevic, P., Bickerton, G. S., Voralek, J., and Talbot, C.:Ground water flow in a
1502 fractured carbonate aquifer inferred from combined hydrogeological and geochemical measurements, Groundwater,
1503 38(3), 350-360, 2000.

1504

1505

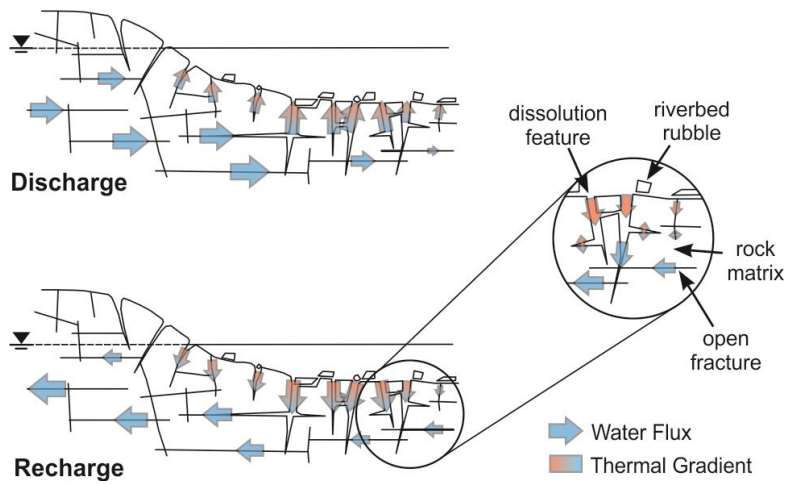
Figures

1506

1507

1508

1509



1510

1511 Figure 1: General conceptual model of the groundwater flow system beneath a fractured bedrock river.

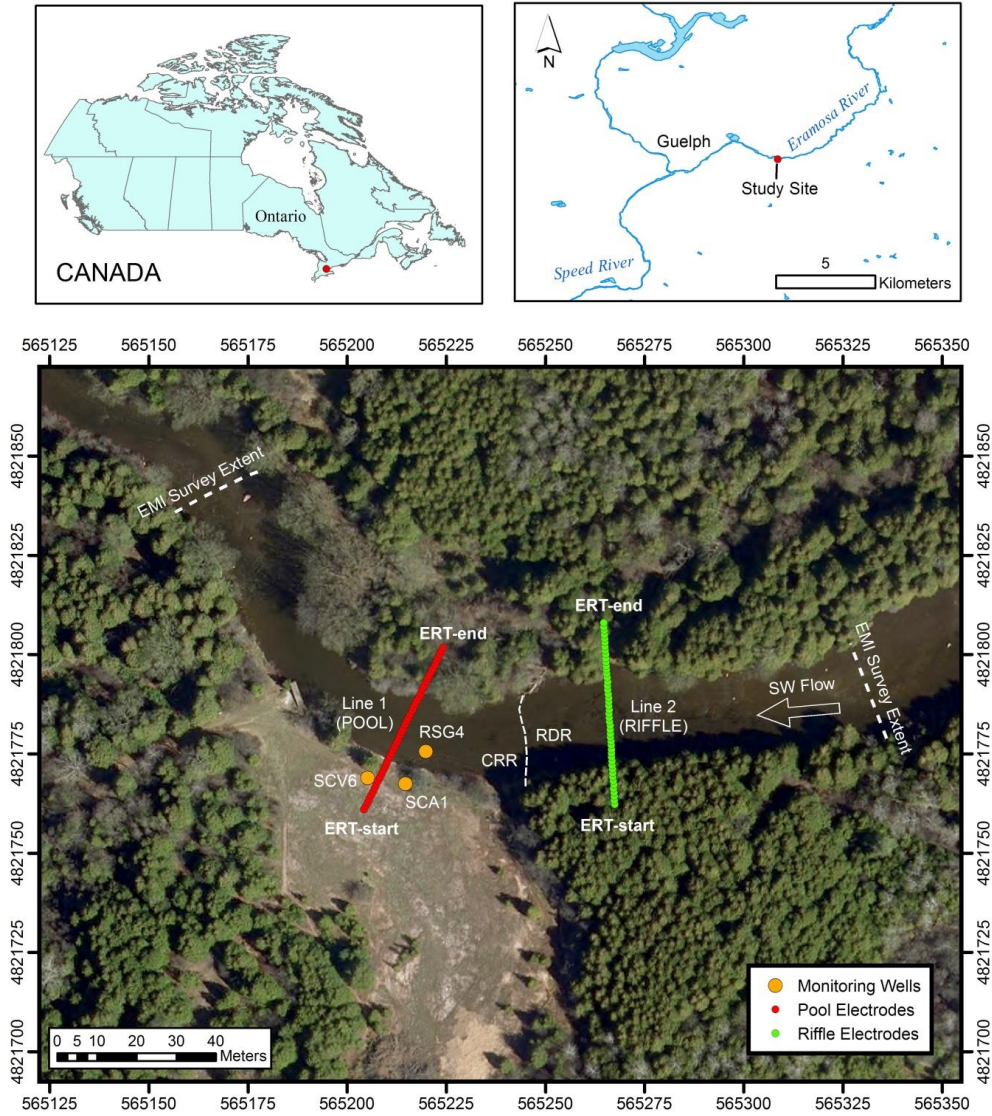
1512 Groundwater-surface water mixing is controlled by open fractures and dissolution-enhanced features with secondary

1513 exchanges (flux or diffusion) occurring between fractures and rock matrix.

1514

1515

1516



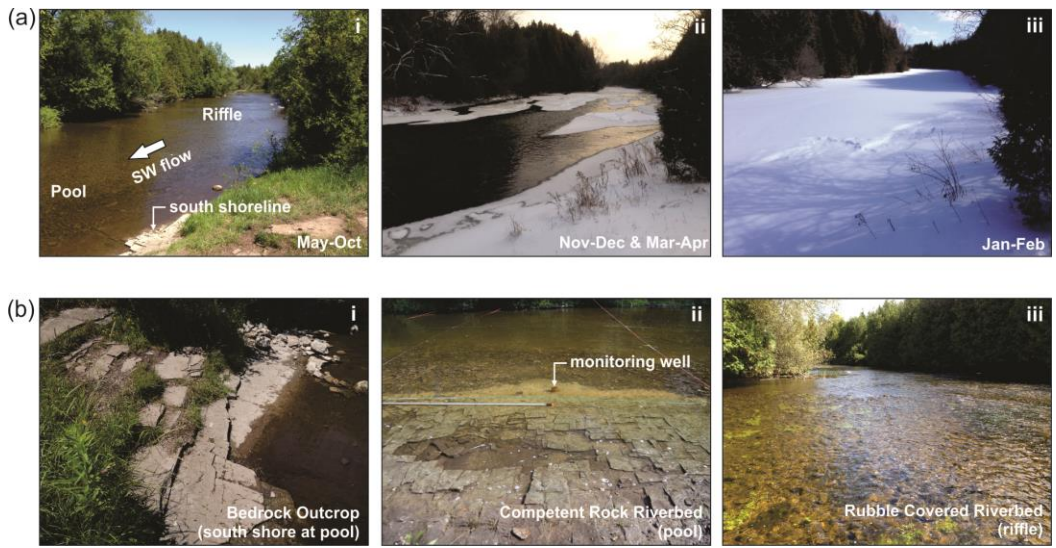
1517

1518 Figure 2: Field site located along the Eramosa River near Guelph, Ontario, Canada. The spatial extent of the
 1519 electromagnetic induction (EMI) surveys, coreholes and groundwater-surface water monitoring points, and fixed
 1520 electrical resistivity tomography (ERT) transects are shown relative to the riffle-pool sequence. The riverbed is
 1521 described as either rubble dominated riverbed (RDR) or competent rock riverbed (CRR) surface.

1522

Deleted: Field site located along the Eramosa River near Guelph, Ontario, Canada. Corehole and monitoring points are shown with fixed electrical resistivity transects located over a pool and riffle. The riverbed is described as either rubble dominated riverbed (RDR) or competent rock riverbed (CRR) surface.

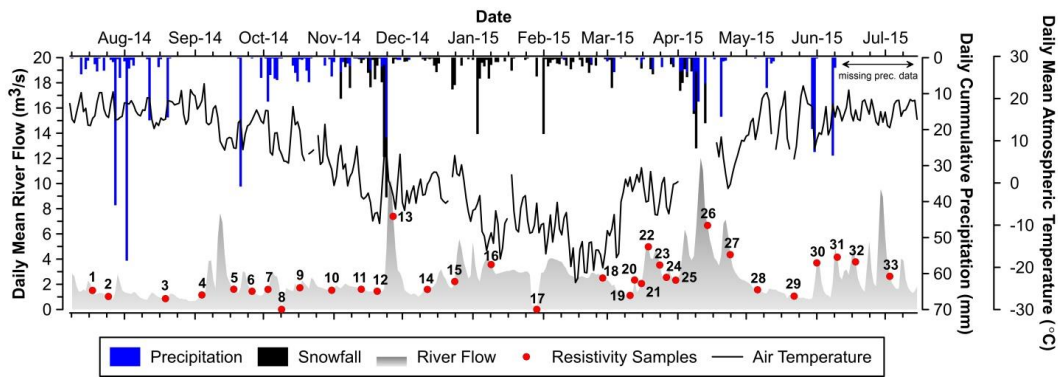
1531
1532
1533
1534
1535



1536
1537
1538
1539

Figure 3: (a) Images of the river during monitored study period. (b) Examples of vertical and horizontal fracturing within pool and rubble covered portions of the riverbed bedrock.

1540
1541
1542
1543
1544
1545

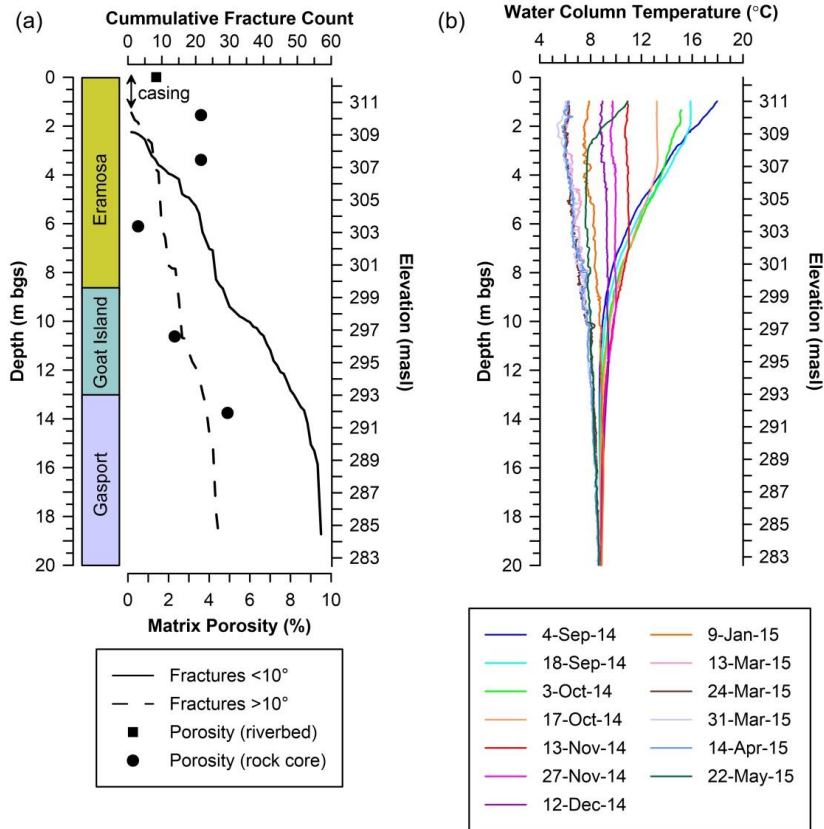


1546
1547
1548
1549
1550

Figure 4: Continuously monitored atmospheric conditions and river flow from Watson Gauge during the study period with superimposed resistivity geophysical measurement events between 18-Jul-2014 and 3-Jul-2015. Note: snowfall is presented as snow water equivalent.

Deleted: flux
Deleted: discrete

1553
1554
1555
1556



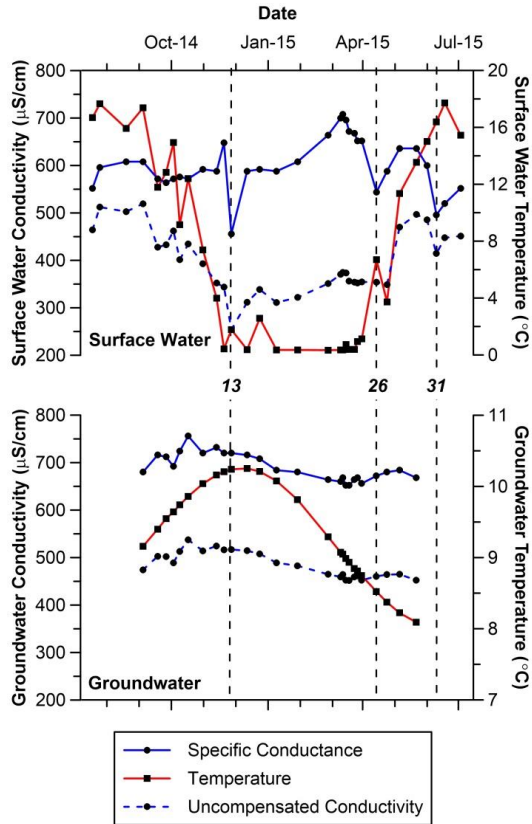
1557

1558 **Figure 5:** (a) Interpreted rock core from SCA1 (angled corehole plunging at 60° with an azimuth of 340°). Fracture
1559 frequency and orientations were obtained using an acoustic televiewer log, while matrix porosity measurements
1560 were obtained from subsamples of the continuous core. (b) Corehole temperature profiles of the SCA1 Flute™
1561 sealed water column.

Deleted: Figure 6

1562

1564



1565

1566 | **Figure 6:** Specific conductance, temperature and uncompensated aqueous conductivity of surface water at RSG4 and
1567 groundwater at the bottom of SCV6 (10.5 m bgs). Uncompensated conductivity represents the actual conductivity
1568 of the porewater after re-incorporating the effect of temperature using the sensors internal temperature-conductivity
1569 correction factor.

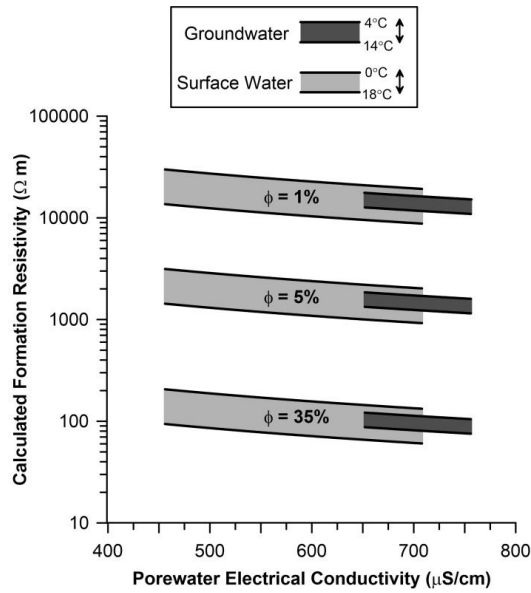
Deleted: Figure 7

1570

1572

1573

1574



1575

1576 **Figure 7:** Calculated formation resistivity based on Eq. (1) and measured variations in surface water and
 1577 groundwater electrical conductivity including **effects of temperature based on** Eq. (2). A cementation factor of 1.4
 1578 was used to represent the fractured dolostone bedrock. Measured water conductivity and temperature were obtained
 1579 from CTD-Diver™ sensors deployed in RSG4 (surface water) and SCV6 (groundwater at a depth of 8 m bgs), and
 1580 the continuous RBR™ temperature profiles shown in **Fig. 5b**. These data show the potential range in formation
 1581 resistivity based on the measured range in specific conductance and **along with the potential impact of** temperature
 1582 **for three different porosity values.** Porosities of 1 % and 5 % correspond to the range measured in the core, while a
 1583 value of 35 % would be representative of a rubble zone.

Deleted: Figure 8

Deleted: potential

Deleted: effects

Deleted: based on

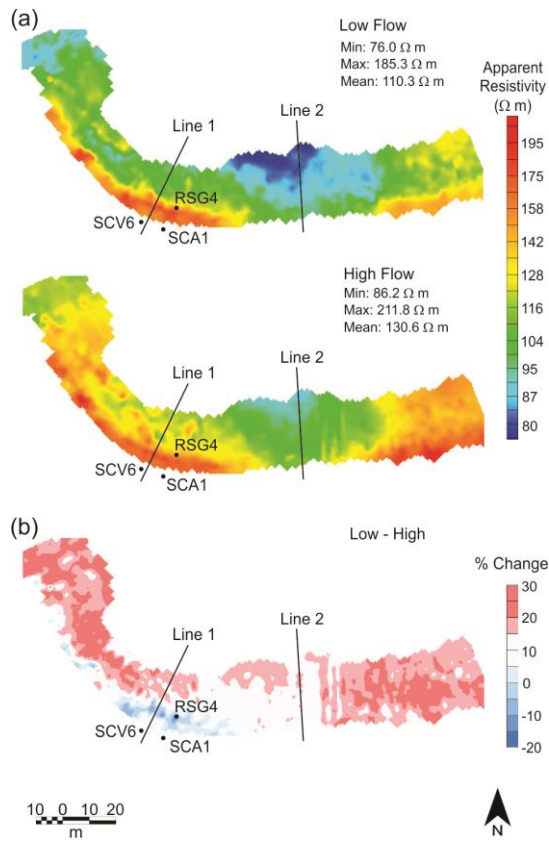
Deleted: Fig. 6

Deleted:

1584

1591

1592

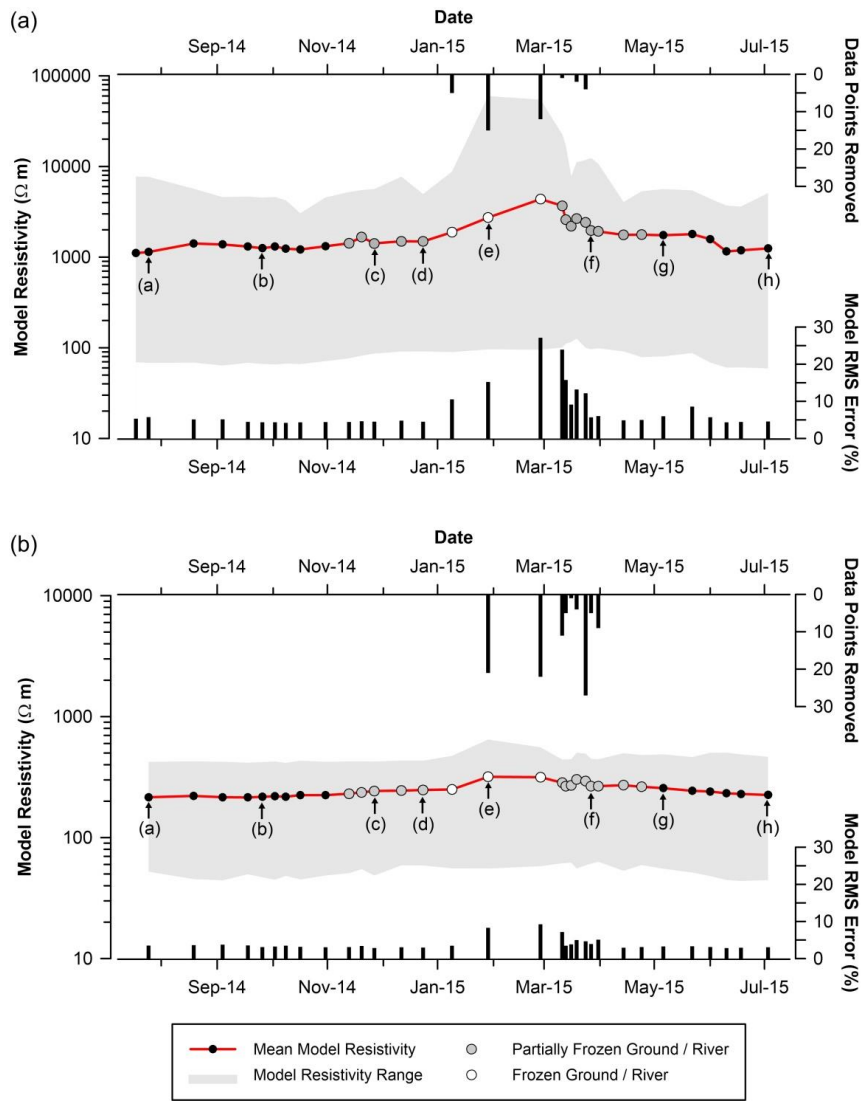


1593

1594 Figure 8: Riverbed resistivity obtained using an EM-31 ground conductivity meter during low-flow/low-stage
1595 conditions on 7-Jul-2014 and high-flow/high-stage conditions on 3-Apr-2013. (b) Percentage change in apparent
1596 resistivity from low to high stage periods.

Deleted: Figure 9

Deleted: Riverbed resistivity obtained using an EM-31 ground conductivity meter during (a) high-flow/high-stage conditions on 3-Apr-2013 and (b) low-flow/low-stage conditions on 7-Jul-2014. ¶



1603

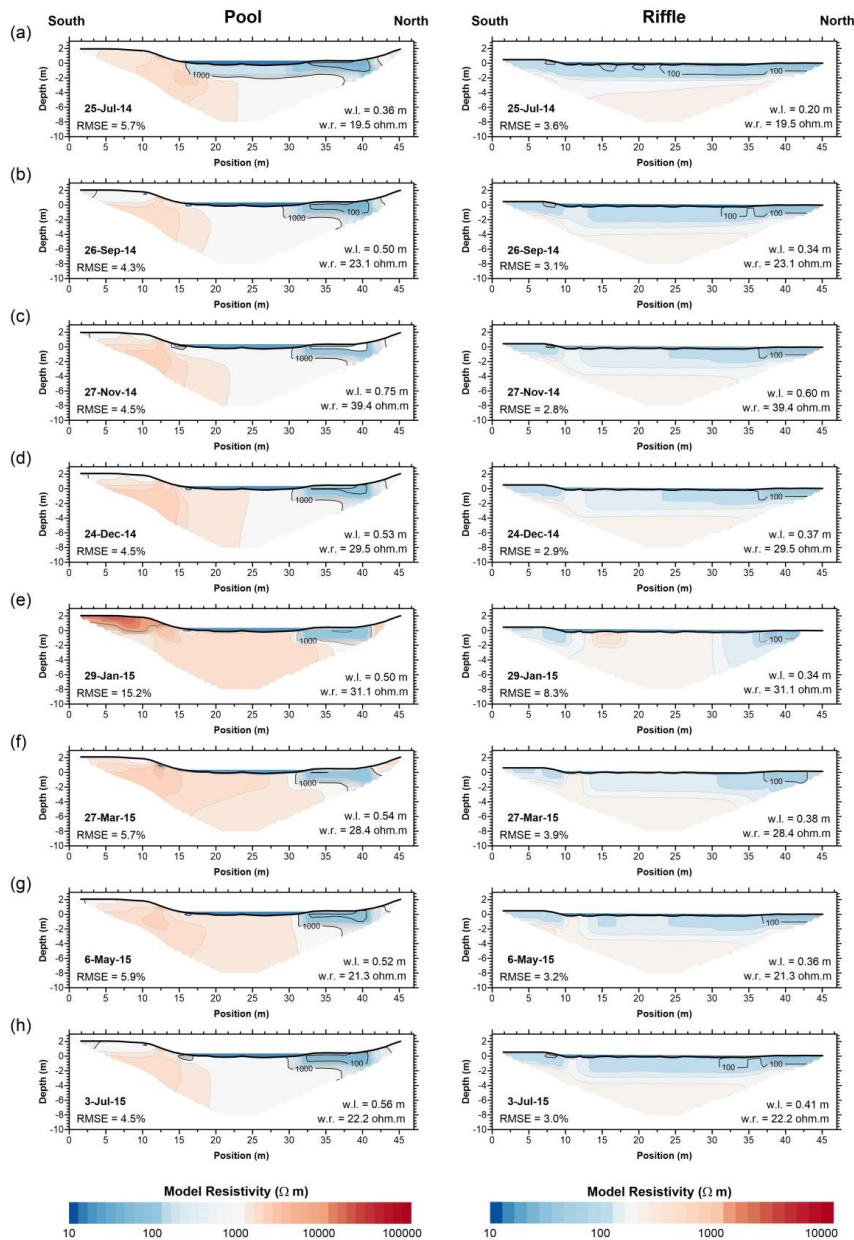
1604 **Figure 9:** Temporal variations in inverted resistivity models for **(a)** pool and **(b)** riffle. Black dots represent unfrozen
 1605 conditions, grey dots indicate partially frozen conditions, while white dots indicate completely frozen river conditions.

Deleted: Figure 10

1606 Select resistivity models (a-h) along the time series are shown in **Fig. 10**.

Deleted: Fig. 11

1607



1610

1611 **Figure 10:** Representative inverse resistivity models across the pool and riffle orientated from south to north.

Deleted: Figure 11

1612 Datasets (a-h) are identified in **Fig. 9**. River stage (w.l.) and surface water resistivity (w.r.) values were fixed in the

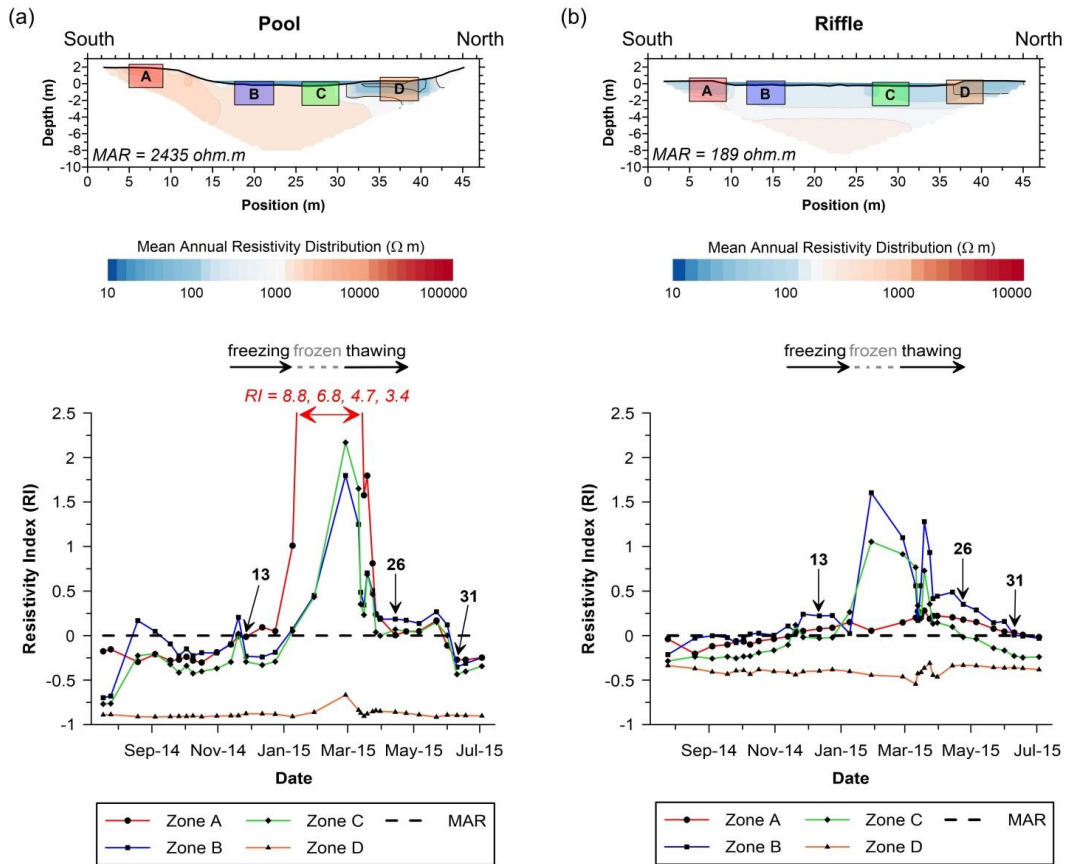
Deleted: Fig. 10

1613 inverse model. A marked increase in resistivity was observed beneath the river during colder seasonal conditions

1614 (November through March), while lower resistivities were observed during warmer seasonal conditions (July).

1615

1618
 1619
 1620
 1621



1622

1623 **Figure 11:** Spatiotemporal fluctuations in resistivity within the focused monitoring zones A, B, C and D. The
 1624 resistivity index (RI) was calculated using Eq. (3), using the mean zone resistivity (MZR) for a given measurement
 1625 date and the mean annual resistivity (MAR) of the whole profile.

Deleted: Figure 12